Aeroelastic and Structures
Research Laboratory
ASRL Technical Report No.74-4

SUBSONIC FLUTTER OF PANELS ON CONTINUOUS ELASTIC FOUNDATIONS - EXPERIMENT AND THEORY

John Dugundji
Earl Dowell
Brian Perkin

MASSACHUSETTS INSTITUTE OF TECHNOLOGY
AEROELASTIC AND STRUCTURES RESEARCH LABORATORY

April 1962

AIR FORCE OFFICE OF SCIENTIFIC RESEARCH
UNITED STATES AIR FORCE
CONTRACT NO. AF 49(638)-219

BIBLIOGRAPHICAL CONTROL SHEET

1. Originating agency and monitoring agency

   O.A.: Massachusetts Institute of Technology, Cambridge, Massachusetts

   M.A.: Office of Scientific Research, United States Air Force

2. Originating agency and monitoring agency report numbers:

   O.A.: M.I.T. Aeroelastic and Structures Research Laboratory Technical Report 74-4

   M.A.: OSR Technical Report

3. Title and Classification:

   SUBSONIC FLUTTER OF PANELS ON CONTINUOUS ELASTIC FOUNDATIONS - EXPERIMENT AND THEORY (UNCLASSIFIED)

4. Personal Authors:

   Dugundji, John, Dowell, Earl, and Perkin, Brian

5. Date of Report: April 1962

6. Pages: viii, 79

7. Illustrative Material: 28 figures

8. Prepared for Contract No.: AF 49(638)-219

9. Security Classification: UNCLASSIFIED

10. Distribution Limitations: None

11. Abstract: The subsonic aeroelastic stability of a two-dimensional panel resting on a continuous elastic foundation was investigated both experimentally and theoretically.

Experimentally, tests were conducted on a 104 in. x 24 in. x 0.018 in. rectangular aluminum panel in a low-speed wind tunnel. Definite flutter of a travelling wave type was observed. Films and oscillograph records were taken.

Theoretically, a finite panel, two mode, standing-wave analysis was shown to give essentially the same behavior as the infinite panel, travelling-wave analysis of Miles (Ref.1) for this panel on an elastic foundation. Although a mild, divergence-type instability exists for these panels, the dominant instability was shown to be of a travelling wave, flutter type. The role of additional internal damping was investigated and found to have an interesting destabilizing effect between the divergence and flutter speeds.

Comparison of experiment and theory showed good agreement in the prediction of the flutter speed and wavelength, but rather poor agreement in the wave speed and frequency at flutter. This discrepancy was attributed to various limitations in the test set-up as well as to the general difficulty of predicting the wave speed and frequency as accurately as the flutter speed.

The present investigation should be of interest in problems of hydroelasticity, axially symmetric cylinders, and inflatable structures at low speeds, as well as to the general problem of panels lying on springy elastic materials.

ACKNOWLEDGEMENT

This report was made within the Aeroelastic and Structures Research Laboratory under United States Air Force Contract No. AF 49(638)-219. The project is administered by Mr. Howard S. Wolko of the Air Force Office of Scientific Research, United States Air Force. A small amount of preliminary work was also done earlier on Contract No. AF 49(638)-933.

The authors wish to acknowledge helpful discussions with Professors Holt Ashley and Marten Landahl on certain phases of this report. The test panel was constructed in the Aeroelastic and Structures Research Laboratory Model Shop under the able direction of Mr. Oscar Wallin, and was tested in the Wright Brothers Wind Tunnel with the assistance of John Stevens and Allan Shaw. The manuscript was typed by G.Hubbard and the figures were prepared by James Shea. The authors express their thanks to all of these people.

SUMMARY

The subsonic aeroelastic stability of a two-dimensional panel resting on a continuous elastic foundation was investigated both experimentally and theoretically.

Experimentally, tests were conducted on a 104 in. x 24 in. x 0.018 in. rectangular aluminum panel in a low-speed wind tunnel. Definite flutter of a travelling wave type was observed. Films and oscillograph records were taken.

Theoretically, a finite panel, two mode, standing-wave analysis was shown to give essentially the same behavior as the infinite panel, travelling-wave analysis of Miles (Ref.1) for this panel on an elastic foundation. Although a mild, divergence-type instability exists for these panels, the dominant instability was shown to be of a travel ling wave, flutter type. The role of additional internal damping was investigated and found to have an interesting destabilizing effect between the divergence and flutter speeds.

Comparison of experiment and theory showed good agreement in the prediction of the flutter speed and wavelength, but rather poor agreement in the wave speed and frequency at flutter. This discrepancy was attributed to various limitations in the test set-up as well as to the general difficulty of predicting the wave speed and frequency as accurately as the flutter speed.

The present investigation should be of interest in problems of hydroelasticity, axially symmetric cylinders, and inflatable structures at low speeds, as well as to the general problem of panels lying on springy elastic materials

TABLE OF CONTENTS

LIST OF SYMBOLS

A		Amplification factor (infinite panel)
$\tilde{A}$		Amplification factor (finite panel)
A_0, A_2, A_4		Constants
B		Damping constant
c		Wave speed relative to air at rest
$c + U$	=	$\bar{c}$ = wave speed relative to panel
c_o		Wave speed in vacuum
D	=	$Eh^3/12(1 - \nu^2)$ = Plate flexural rigidity
(D.R.)		Damping ratio
E		Modulus of elasticity
f_1		Correction factor given by Eq.22
f_2		Mode factor given by Eq.59
G	=	$B\lambda/2\pi mU$ = nondimensional damping
h		Plate thickness
i	=	$\sqrt{-1}$
K		Spring stiffness of elastic foundation
$\bar{K}$	=	$K\ell^4/D$ = nondimensional spring stiffness parameter
ℓ		Length of panel
m		Mass of panel per unit area
n		Mode number
p		Pressure
p_∞		Pressure of air at free stream

q_n		Generalized coordinate
Q	=	$\rho_\infty U^2 \ell^3/D$ = nondimensional dynamic pressure parameter
s		Root of characteristic equation (actual time)
$\bar{s}$	=	$s/\sqrt{D/m\ell^4}$ = root of characteristic equation (nondimensional time)
t		Time
$\bar{t}$	=	$t\sqrt{D/m\ell^4}$ = nondimensional time
u	=	$\sqrt[4]{(m\omega^2 - K)/D}$
U		Air speed at free stream
w		Deflection of plate
x		Coordinate
Δp	=	Differential pressure loading over panel
ϵ		Phase angle
ζ	=	c/U
ζ_o	=	c_o/U
λ		Wavelength
μ	=	$\rho_\infty \lambda/m2\pi$ = mass density ratio (infinite panel)
$\tilde{\mu}$	=	$\rho_\infty \ell/m\pi$ = mass density ratio (finite panel)
ν		Poisson's ratio
ξ		Coordinate
ρ_∞		Density of air at free stream
φ_n		n^{th} free vibration mode
ω		Frequency

1. INTRODUCTION

The problem considered here is the aeroelastic stability of a long panel resting on a continuous elastic foundation. Such a situation might arise for a panel, lying on some springy insulating material, exposed to an air flow over its top side.

The theory of Miles in Ref.1 for infinitely long panels can readily be adapted to describe this behavior. In this theory, unstable travelling waves are predicted above a critical flutter speed for both the subsonic and supersonic cases. For panels resting on an elastic foundation, these unstable travelling waves possess a finite wavelength, and hence give the possibility of actually viewing these waves on a long panel. Accordingly, it was decided to build such a panel and test it in a conveniently available low-speed wind tunnel. It was hoped to shed some light on the travelling wave versus standing wave theories of panel flutter, and also to reinvestigate the possibility of panel flutter at subsonic speeds.

The present report gives an account of the experiments performed, and a detailed theoretical analysis of the panel from both the infinite length and finite length point of view. Some earlier preliminary work in this general area was done by Dowell in Ref.2.

The results of the present investigation may also be of interest in the related problems of hydroelastic panel flutter, axially symmetric cylinder flutter at low speeds, and panel flutter of inflatable structures at low speeds.

2. EXPERIMENT

2.1 Panel Test Model

The model to be tested consisted basically of a flat rectangular sheet of aluminum 2024-T3 with dimensions* 104 in. x 24 in. x 0.018 in. The panel was orthogonally stiffened by a series of aluminum angle stiffeners, spaced 1.58 inches apart, and running perpendicular to the long edges of the panel. The panel was attached to a rigid wooden box frame by resting on three rows of helical springs running parallel to the long edges of the panel, and by a plastic hinge along one of the short sides (the leading edge of the panel). The two long edges of the panel were left free, while the other short side (the trailing edge) was left free during some of the tests, and pinned during others. A sketch of the panel and its support system is shown in Fig.1.

Both the aluminum angle stiffeners and the helical coil springs were attached to the aluminum sheet by Armstrong A-2 epoxy resin glue. This provided a strong and rugged bond. The angle stiffeners were used in order to insure two-dimensional behavior of the panel.** The springs in each of the three rows were spaced 1.58 inches apart in the stream direction. Since the wavelengths anticipated were of the

*During the early part of the test program (Run 17), the very rear part of the panel was damaged. The panel was then shortened from 104 in. to 93 in. for the remainder of the tests.

**An oil-can effect existed originally in the forward part of the sheet. This necessitated somewhat larger size stiffeners in this vicinity in order to get rid of this three-dimensional effect.

order of 24 inches, it was felt that the discrete springs adequately represented a continuous elastic foundation.

The leading edge was pinned by a mylar strip hinge. The trailing edge, which was kept free for much of the test program, was limited to about 1/2 in. vertical motion above the undeformed position by three loosely fitting bolts. These were placed in after Run 17, when excessive motion damaged the trailing edge. During the latter part of the test program, the trailing edge was pinned instead of free. This was provided by replacing the three loosely fitting bolts by three plastic knife edges. Slotted holes were made in the panel to prevent axial tension forces from developing when the panel deflected vertically.

The bottom of the wooden box frame was covered by a wooden panel with numerous one-inch diameter holes to allow tunnel static pressure to be developed on the inside of the aluminum test panel.

A square grid of black lines was painted on the panel, for ease in viewing and observing the panel behavior. The distance between lines was roughly six inches, and the lines perpendicular to the flow were numbered from 0 to 16, starting at the leading edge. Eight SR-4 strain gages were also placed on the underside of the panel near its midsection. These were to be used to obtain frequency and phasing behavior. The location of the grid and the strain gages is shown in Fig.2.

2.2 Static and Vibration Tests

Prior to flutter testing in the tunnel, static tests were made on a typical helical coil spring, and vibration tests were made of the panel as a whole in its wooden box frame.

The helical coil springs used had a length of 1 1/2 inches, a diameter of 1/2 inch, and could be compressed to bottom without buckling. The results of a static compression and tension test of a typical spring is shown in Fig.3. The spring is seen to be fairly linear over a wide range and has a spring rate of 0.88 lb/in.

The panel was vibrated in its wooden supporting frame, by attaching an electrodynamic shaker to the panel centerline, about 8 inches from the leading edge. The natural modes and frequencies were obtained by visual observation. Salt was sprinkled over the panel to determine the position of the node lines, and the audio oscillator output frequency was checked with a strobotac. The experimental modes and frequencies together with theoretical ones computed from the spring and mass properties (see Section 3.1), are given in Fig.4 for the higher modes (n = 7 to n = 11). The observed frequencies are in reasonable agreement with those calculated. The observed node lines are not as clear cut or uniformly spaced as the theoretical ones. However, they do resemble the calculated ones, and the trends with n are quite good. As can be expected from the theoretical analysis, the lower modes (n = 1, 2, 3, etc.) are too close together to be separately excited and observed by this single shaker.

The panel was also vibrated with the shaker located 16.5 inches from the trailing edge. As these mode shapes and frequencies were quite similar to those obtained with the shaker in the forward position, they are not repeated here.

2.3 Mounting in Tunnel

The test panel and its supporting wooden box frame were mounted in the M.I.T. Wright Brothers low-speed wind tunnel. This tunnel has a 7 1/2 ft x 10 ft elliptical test

section which is vented to approximately atmospheric pressure, and is capable of running to speeds of about 140 mph at atmospheric pressure. The wooden box frame on which the test panel lay, was placed between two end plates extending from the ceiling to about three feet from the floor, as shown in Fig.5. These end plates were used to try to assure two dimensionality of the flow. They were made of 1/2-inch plywood, except for the center portion of one side which was plexiglas in order to allow visual observation of the test panel surface during the flutter run. The wooden box frame could be changed in angle of attack somewhat in order to adjust the pressure and velocity distribution over the panel. Three pitot-static tubes were placed about 12 inches over the centerline of the panel in order to measure the velocity. Later on in the test program, nine more pitot-static tubes were added in order to survey the pressure and velocity distribution over the panel more accurately.

For observing visually the static vertical deflections of the panel under the action of the air forces, a series of six long black lines 1/4-inch apart were ruled on the inside face of one of the wood beams of the supporting wooden box frame. The static vertical deflection of the aluminum panel could then be estimated visually by reading it against this grid.

The panel surface with its six-inch square grid could be viewed visually through the plexiglas end plate and the wind tunnel window. Movies were taken by a 16 mm camera from this position. Also, the eight strain gages on the panel underside were connected to a recording oscillograph.

2.4 Flutter Test Procedure

During a typical flutter test run, the tunnel speed was raised to a given value and held. For this speed, the tunnel pitot-static tube was read. This gave the reference tunnel setting and represented the dynamic pressure in inches of alcohol at some reference point in the tunnel test section. The three pitot-static tubes over the panel itself were then read, in order to obtain the actual velocity at the panel. The static deflection shape of the panel was then recorded by visual observation of the deflections of the long edge of the panel against the ruled 1/4-inch grid on the inside face of the supporting wooden frame. The above test runs were repeated in small tunnel velocity increments until significant vibrational activity or flutter was observed visually over the panel surface. Then, both oscillograph records of the strain gages, and 16 mm movies of the panel surface were taken.

A test log of the different runs carried out is given in Fig.6. This test program is a consequence of attemps to repeat results, to investigate both free and pinned trailing-edge conditions, to minimize the effects of nonuniform pressure and velocity distributions over the panel, and to determine the detailed pressure and velocity distributions over the panel.

During Run 17, the panel trailing edge fluttered violently and as there were no stops at that time, the last nine inches of the panel was damaged. This was subsequently repaired by cutting off the last eleven inches of the panel and installing loosely fitting bolt stops (as mentioned in Section 2a). For the remainder of the tests, the flutter that did occur remained nondestructive.

Early in the test program, a significant static depression occurred near the leading edge of the panel (see Fig.9). This appeared to be attributed to nonuniform pressure and velocity distributions over the panel, and was remedied somewhat by increasing the angle of attack of the panel between the end plates. Later on in the test program (Run 100 and on), more accurate pressure and velocity surveys over the panel were performed using twelve pitot-static tubes in place of the original three.

2.5 Test Results

a) Pressure and Velocity Surveys

The results of pressure and velocity surveys taken during Runs 100 through 125 are shown in Figs.7 and 8. These were obtained for the different angle-of-attack settings and tunnel settings. There was some small scatter in the original data which was traced subsequently to slight leaks in the pressure lines of a few of the pitot-static tubes. The data in Figs.7 and 8 represent the best faired estimate of the pressure and velocity distributions taken six inches above the surface of the panel. There was no significant difference between the distributions six inches above the panel and those twelve inches above the panel. The undesirable variation of the pressure and velocity distributions over the panel surface are to be noted. On the underside of the panel, the pressure distribution was found to be fairly uniform over the entire length of the panel for each given angle-of-attack setting and tunnel setting.

b) Static Deflections

The static deflections of the panel for different angle-of-attack settings and tunnel settings are shown in Fig.9. The prominent depression near the leading edge is

clearly visible. This tended to become smaller for the high angle-of-attack setting. Also clearly visible is a sinusoidal wave pattern of about two-ft wavelength that developed near the trailing edge on many of the runs, particularly on Runs 114 through 121, the low angle of attack, pinned case.

c) Flutter Observations

Flutter was observed for many of the runs. Outside of Run 17, it tended to be nondestructive and limited in amplitude, so that it could be viewed for relatively long periods of time. The double amplitude reached values of one-half inch on many of these runs. The occurrence of flutter is indicated in the test log, Fig.6. These results are summarized in Fig.10. The flutter velocity quoted was taken at 70 inches aft of the leading edge (roughly at 3/4 of the length of the panel).

Considerable variation in the flutter speeds occurred particularly between the different angle-of-attack settings. There was a lesser change between the free and pinned-end conditions. It is felt that the results for the high angle-of-attack case are the most reliable since these had the smallest static depression at the leading edge, and the smallest pressure and velocity variation over the panel surface. The large static depression in addition to aerodynamic effects, shortened the effective length of the panel and may have introduced midplane tension and structural nonlinear effects into the panel behavior.

d) Movies

Movies of many of the flutter test runs were taken with a 16 mm camera at 64 frames/sec. The more interesting shots were compiled together into a single 400-ft film strip

representing 22 different runs. The film log for these pictures is given in Fig.11. The movie films recorded both steady flutter, and the onset of flutter in some cases. Typical flutter film sequences are shown in Figs.12a through 12d for the high and medium angle-of-attack cases. An example of the static, divergence-type phenomenon observed during Runs 114 through 121 is given in Fig.12e.

Analysis of these flutter film sequences and other runs in the film strip seem to indicate a flutter frequency of about 14 cps, a wavelength of about 2 to 2 1/2 feet, and a wave speed of about 35 ft/sec. The waves generally appear to be travelling downstream, although there seems to be some small "sticking" or standing wave component present in some of them. Some small distortion of the travelling waves from a pure sinusoidal shape is evident, particularly for the larger amplitudes of wave motion. A camera speed somewhat faster than the 64 frames/sec used here, would have helped define the wave motion more accurately.

e) Oscillograph Records

Oscillograph records of many of the flutter test runs were taken. The oscillograph log is given together with the film log in Fig.11. Typical oscillograph records for the same runs as the film strips of Figs.12a to 12d are given in Figs.13a through 13d. On these, the eight strain-gage traces are shown, giving clearly the frequency and phasing of the different locations. Since the gages are all roughly similar in sensitivity, a measure of the amplitudes is also obtained for these locations. To compare amplitudes between different oscillograph records, all amplitudes on a given record should be multiplied by the amplitude factor A.F. indicated, in order to adjust roughly for the different amplifier gain settings used during the test program.

The traces shown in Figs.13a through 13d show strong evidences of standing waves with some small travelling-wave components present. The frequencies average 14.4 and 13.7 cps for the high and medium angle-of-attack settings, respectively. The half wavelengths average about four-gage lengths or 12.8 inches. This is particularly clear from Fig.13d.

Two other oscillograph records, from Runs 12 and 76, are shown in Figs.13e and 13f. These were taken slightly below the visually observed flutter, and show here clear evidences of travelling waves.

f) Summary of Results

It appeared that definite flutter was obtained for this panel at speeds of about 95 mph, frequencies of 14.4 cps, wavelengths of about 2 to 2 1/2 feet, and wave speeds of about 35 ft/sec. The waves generally appeared to be travelling downstream although there seemed to be some "sticking" or standing wave components present near the center of the panel. The flutter speed was not affected much by the trailing-edge condition, i.e., whether pinned or free there. Prior to flutter, the panel assumed a sinusoidal static deflection shape of about two feet wavelength in the vicinity of the trailing edge (in one case, Run 121, this became a rather sizable deflection). There also appeared a prominent static depression in the vicinity of the leading edge which was remedied somewhat by altering the angle of attack and hence pressure distribution over the panel.

2.6 Improvement of Experimental Test

After having carried out the above experimental test program, it has become apparent that several improvements can be made to obtain more accurate test data in any

future work along these lines.

First, somewhat larger angle stiffeners should be used to insure two-dimensional behavior of the panel and to eliminate any possible oil-canning effects in the panel behavior.

Second, more care should be given to maintaining uniform pressure and velocity distributions over the panel, and to eliminating the static depression near the leading edge. This could be accomplished by more angle-of-attack manipulation, a longer nosepiece on the wooden box frame, better contouring of the walls above and alongside the panel, and better venting between the upper and lower sides of the panel. A thorough pressure and velocity survey should be made before passing on to the flutter tests.

Third, better observation techniques could be utilized. These would include using a faster frame speed camera, better calibration of the strain gages, accurate synchronization of camera with oscillograph records, and photographing more of the panel surface in the movies.

3. THEORY

3.1 Free Vibration Modes

The equation for the deflection $w(x,t)$ of a two-dimensional panel resting on a continuous elastic foundation is,

$$D\frac{\partial^4 w}{\partial x^4} + Kw = \Delta p - m\frac{\partial^2 w}{\partial t^2} \tag{1}$$

where for the present panel,

$$\begin{aligned} D &= \frac{Eh^3}{12(1-\nu^2)} = \text{flexural rigidity} = 5.61 \text{ lb-in} \\ K &= \text{foundation stiffness} = 0.0696 \text{ lb/in}^3 \\ m &= \text{mass per unit area} = 5.79 \times 10^{-6} \text{ lb-sec}^2/\text{in}^3 \\ \Delta p &= \text{pressure loading} = \text{lbs/in}^2 \\ \ell &= \text{length of panel} = 104 \text{ in} \\ \rho_\infty &= \text{air density at sea level} = 0.1148 \times 10^{-6} \text{ lb-sec}^2/\text{in}^4 \end{aligned} \tag{2}$$

For free vibrations in a vacuum, the pressure loading is assumed zero. Upon utilizing the standard separation of the variables technique, one arrives at the general solution,

$$w(x,t) = A\sin(\omega t + \epsilon)\left\{C\cosh ux + D\sinh ux + E\cos ux + F\sin ux\right\} \tag{3}$$

where

$$u = \sqrt[4]{\frac{m\omega^2 - K}{D}} \tag{4}$$

Putting in the boundary conditions,

$$@\ x = 0 \begin{cases} w = 0 \\ \dfrac{\partial^2 w}{\partial x^2} = 0 \end{cases} \qquad @\ x = \ell \begin{cases} \dfrac{\partial^2 w}{\partial x^2} = 0 \\ \dfrac{\partial^3 w}{\partial x^3} = 0 \end{cases}$$

one obtains the characteristic equation,

$$\tan u\ell = \tanh u\ell \tag{5}$$

Solving the above for $u\ell$, and making use of Eq.4, the following natural frequencies are obtained,

$$\omega_n = \sqrt{\frac{K}{m} + (n+\tfrac{1}{4})^4 \frac{\pi^4 D}{m\ell^4}} \tag{6}$$

The corresponding natural mode shapes $\varphi_n(x)$ are,

$$\phi_n(x) = \sin(n+\tfrac{1}{4})\frac{\pi x}{\ell} + \frac{.7071\,(-1)^n}{\sinh(n+\tfrac{1}{4})\pi} \sinh(n+\tfrac{1}{4})\frac{\pi x}{\ell} \tag{7}$$

For the higher values of n, these modes resemble pure sine waves except in the immediate vicinity of the trailing edge. The n^{th} mode has n node lines spaced approximately a distance $\ell/(n + 1/4)$ apart, starting from the leading edge.

For the present panel, the theoretical frequencies and node lines for free vibrations in a vacuum are shown in Fig.4, corresponding to values of n = 7 to n = 11. The fundamental frequency for n = 1 is calculated at 17.5 cps. It is seen that the lower modes are spaced very close together in frequency.

For the actual vibrations of the panel in still air, an additional virtual mass of air should be included with the panel mass. This is shown in Section 3.3 to result in a total mass* of approximately,

$$m\left(1 + 2\frac{\rho_a \ell}{m\pi n}\right) = m\left(1 + \frac{1.312}{n}\right) \tag{8}$$

These still air frequencies are also shown in Fig.4. The mode shapes are unchanged by this additional air mas.

---

*For still air on both sides of the panel. Also for high n, where sin $n\pi x/\ell$ is a reasonable approximation to the mode shape.

3.2 Infinite Panel in Incompressible Flow

a) No Internal Damping

The flutter of an infinite panel in two-dimensional incompressible flow has been investigated by Miles in Ref.1. He utilizes there an axis system which is fixed to the air at rest, and considers the infinite panel to be moving with velocity U in the negative x direction. The equation of motion for such an undamped panel on an elastic foundation is,

$$D\frac{\partial^4 w}{\partial x^4} + Kw + m\left(\frac{\partial}{\partial t} - U\frac{\partial}{\partial x}\right)^2 w = \Delta p \qquad (9)$$

Miles has shown that for travelling wave solutions of the form,

$$w(x,t) = w_o\, e^{i\frac{2\pi}{\lambda}(ct - x)} \qquad (10)$$

the aerodynamic pressure distribution for air acting on the top side of the panel only,* is

$$\Delta p = \rho_\infty \frac{2\pi}{\lambda} c^2 w_o\, e^{i\frac{2\pi}{\lambda}(ct - x)} \qquad (11)$$

Substituting Eqs.10 and 11 into Eq.9, one is lead to the equation

$$(\zeta + 1)^2 - \zeta_o^2 + \mu\zeta^2 = 0 \qquad (12)$$

where

---

*The pressure acting on the bottom side of the panel is assumed constant at p_∞ in the present analysis. The presence of air on the bottom side of the panel is examined in Appendix A and is found to be small for the low μ's of interest here.

$$\zeta = \frac{c}{U} \tag{13}$$

$$\zeta_o = \frac{c_o}{U} \tag{14}$$

$$\mu = \frac{\rho_\infty \lambda}{2\pi m} \tag{15}$$

$$c_o = \sqrt{\frac{K}{m}\left(\frac{\lambda}{2\pi}\right)^2 + \frac{D}{m}\left(\frac{2\pi}{\lambda}\right)^2} \tag{16}$$

In the above quantities, c represents the wave speed with respect to the air at rest, c_o represents the wave speed in the absence of air ($U = 0$, $\rho_\infty = 0$), and μ represents the mass density ratio of the panel* (for air on one side of the panel only). Equation 12 is solved for ζ. Any solutions for ζ having negative imaginary parts represent instabilities.

Solving Eq.12 explicitly for ζ, Miles obtains the following expressions for the wave speed relative to still air, c,

$$c = \frac{1}{1+\mu}\left\{-U \pm \sqrt{(1+\mu)c_o^2 - \mu U^2}\right\} \tag{17}$$

and for the wave speed relative to the panel, c + U,

$$c + U = \frac{1}{1+\mu}\left\{\mu U \pm \sqrt{(1+\mu)c_o^2 - \mu U^2}\right\} \tag{18}$$

It is readily seen from these expressions that negative imaginary values of c, hence instability, will occur for

*Note this definition of μ is the reciprocal of another definition of mass density ratio frequently used in flutter work.

$$\frac{U}{c_o} > \sqrt{\frac{1+\mu}{\mu}} \tag{19}$$

The above criterion is plotted in Fig.14. The corresponding wave speed relative to the panel is,

$$c + U = \frac{\mu}{1+\mu} U \tag{20}$$

In applying the above criterion, it is to be noted that both μ and c_o are functions of the wavelength λ. Hence, one must investigate the variation of flutter speed with wavelength. For a panel on an elastic foundation, the variation of c_o with λ is given by Eq.16 and is shown plotted in Fig.15. The corresponding variation of flutter speed U_F with λ is shown in Fig.16. Unlike the case of a membrane or a plate where the minimum flutter speed occurs for $\lambda \to \infty$, the panel on an elastic foundation possesses a minimum flutter speed at a finite value of λ and thereby gives hopes of actually seeing these travelling waves on a long panel. This wavelength λ for the minimum flutter speed is given by

$$\lambda_{min} = 2\pi \left(\frac{D}{K}\right)^{1/4} f_1 \tag{21}$$

where f_1 is a correction factor given by

$$f_1 = \left(\frac{1.5+\mu}{.5+\mu}\right)^{1/4} \tag{22}$$

and is seen to vary from $f_1 = 1.0$ at high values of μ to $f_1 = 1.316$ as $\mu \to 0$.

For the present panel, the characteristics at flutter are calculated numerically as

Flutter speed $U_F = 105.5$ mph

Wavelength $\lambda = 25$ in

Wave speed $c + U = 11.4$ ft/sec (23)

Frequency $\omega = \frac{2\pi}{\lambda}(c + U) = 34.4$ rad/sec $= 5.5$ cps

Density ratio $\mu = 0.079$

Below the flutter speed, a multitude of undamped travelling wave solutions are possible corresponding to different wavelengths λ. The wave speeds relative to the panel, $c + U$, are plotted in Fig.17 for different wavelengths. These were computed from Eq.18.

It is of interest to investigate the unstable behavior of the panel above the flutter speed and to determine how fast the instability sets in. In terms of a coordinate system $\bar{x}$ fixed to the moving panel, the travelling wave solutions of Eq.10 can be written

$$W(\bar{x},t) = W_o\, e^{i\frac{2\pi}{\lambda}\left([c_R+U]t-\bar{x}\right)}\, e^{-\frac{2\pi}{\lambda}c_I t} \tag{24}$$

where c_R and c_I are the real and imaginary parts respectively of c. The quantity $(c_R + U) = (c + U)_R$ represents the wave speed relative to the panel, while the quantity $c_I = (c + U)_I$ is related to the rate of growth of the waves as they move along the panel. As a quantitative measure of this rate of growth, the amplification A is introduced. This amplification A is defined as the ratio of the wave amplitudes during the time it takes the wave to travel one wavelength λ (i.e., $A = 2 \rightarrow$ wave doubles, etc.). From Eq.24 it can be deduced that,

$$A = e^{-2\pi \frac{c_I}{c_R + U}} \qquad (25)$$

Introducing the results from Eq.18 into the above gives,

$$A = e^{+\frac{2\pi}{\sqrt{\mu}}\sqrt{1 - \frac{1+\mu}{\mu}\left(\frac{c_R}{U}\right)^2}} \qquad (26)$$

For this panel, the complex wave speed c + U is shown plotted in the complex plane in Fig.18 for various speeds and wavelengths λ. The corresponding amplification A is given in Fig.19 also for various speeds and wavelengths. It can be seen that the instability sets in very sharply after U_F is exceeded, and the amplification A reaches values of the order of 100 for 2 or 3 mph above the flutter speed.

b) Internal Damping Present

The preceding analysis was for a panel with no internal damping present in the structure. Next, consider the effect of adding some internal damping to the structure. The basic equation of motion would then be,

$$D\frac{\partial^4 w}{\partial x^4} + Kw + m\left(\frac{\partial}{\partial t} - U\frac{\partial}{\partial x}\right)^2 w + B\left(\frac{\partial}{\partial t} - U\frac{\partial}{\partial x}\right)w = \Delta p \qquad (27)$$

and the corresponding equation in ζ would read

$$(\zeta + 1)^2 - \zeta_0^2 + \mu\zeta^2 - i\frac{B\lambda}{2\pi m U}(\zeta + 1) = 0 \qquad (28)$$

Solving the above equation for ζ now gives

$$(1+\mu)\zeta = -1 + i\frac{G}{2} \pm \sqrt{\left[\zeta_o^2(1+\mu) - \mu - \frac{G^2}{4}\right] + i\,\mu G} \qquad (29)$$

where $G = B\lambda/2\pi mU$ is a measure of the additional damping present in the structure. Unstable solutions will now occur if the imaginary part of the radical has an absolute value greater than G/2.

The imaginary and real parts of the above radical can be evaluated as

$$Im\{\sqrt{\ }\} = \pm\frac{1}{\sqrt{2}}\sqrt{+\sqrt{\left[\zeta_o^2(1+\mu) - \mu - \frac{G^2}{4}\right]^2 + [\mu G]^2} - \left[\zeta_o^2(1+\mu) - \mu - \frac{G^2}{4}\right]} \qquad (30)$$

$$Re\{\sqrt{\ }\} = \frac{\mu G}{2\,Im\{\sqrt{\ }\}} \qquad (31)$$

Unstable solutions will appear for

$$\frac{G}{2} < \frac{1}{\sqrt{2}}\sqrt{+\sqrt{\left[\zeta_o^2(1+\mu) - \mu - \frac{G^2}{4}\right]^2 + [\mu G]^2} - \left[\zeta_o^2(1+\mu) - \mu - \frac{G^2}{4}\right]} \qquad (32)$$

By routine algebraic manipulation, the above inequality reduces simply to,

$$\zeta_o^2 < \mu \qquad (33)$$

At the value $\zeta_o^2 = \mu$, it can be shown by direct substitution that $Im\{\sqrt{\ }\} = \pm G/2$. It is interesting to note that the above criterion Eq.33 does not depend on the magnitude of the damping G present in the structure. Hence for any small amount of damping present instability will set in for

$$\frac{U}{c_o} > \sqrt{\frac{1}{\mu}} \qquad (34)$$

rather than the somewhat higher value given previously by Eq.19 for the completely undamped case. This new criterion is shown plotted in Fig.14 together with the previous criterion for the undamped panel. The difference between the two criteria increases for increasing μ. At the onset of this new instability, the Re $\{\sqrt{\ }\} = -\mu$, and one obtains from Eq.29 the wave speed relative to the panel $c + U$ as,

$$c + U = 0 \qquad (35)$$

This indicates a static divergence-type instability rather than a travelling wave flutter-type instability as obtained in the undamped case.

The presence then, of even a very small amount of internal damping is sufficient to lower the instability speed of the panel and to change its character from a travelling wave flutter-type instability to a static divergence-type instability. This behavior has been noted also by other authors, for example, Leonard and Hedgepeth in Ref.3 for the similar case of thin circular cylinders in an airstream, and also more recently by Landahl in Ref.4 in a study of the boundary layer on a flexible panel.

To apply the criterion given by Eq.34, one must investigate the variation of the instability speed with wavelength λ, as was done for the undamped case. This divergence speed is shown plotted in Fig.16 together with the previous flutter speed for the undamped panel. The wavelength λ for the minimum divergence speed is given by Eq.21 with the correction factor $f_1 = 1.316$.

For the present panel with a slight amount of damping present, the characteristics at instability (divergence now) are calculated numerically as

$$\begin{aligned} &\text{Divergence speed } U_D = 101.5 \text{ mph} \\ &\text{Wavelength } \lambda = 25 \text{ in} \\ &\text{Wave speed } c + U = 0 \\ &\text{Frequency } \omega = 0 \\ &\text{Density ratio } \mu = 0.079 \end{aligned} \tag{36}$$

The above divergence speed is somewhat lower than the previous undamped panel flutter speed of 105.5 mph. Below the above divergence speed, the travelling wave solutions corresponding to different wavelengths are all damped travelling waves.

It is again of interest to investigate the unstable behavior of the panel above the divergence speed and to determine how fast this instability sets in. The amount of internal damping present in the panel foundation can be more conveniently expressed as

$$B = 2\,(D.R.)\sqrt{K\,m} \tag{37}$$

where (D.R.) represents the familiar critical damping ratio and is of the order of 0.01 for this metallic structure. Using Eq.37, the damping parameter G of Eqs.29 to 32 becomes

$$G = \frac{(D.R.)}{\pi}\frac{\lambda}{U}\sqrt{\frac{K}{m}} \tag{38}$$

For the present panel, the complex wave speed $c + U$ was computed from Eqs.29 to 32 for speeds above di-

vergence, and for several values of damping ratio (D.R.). The results are shown plotted in the complex plane in Fig. 20. The corresponding amplification A is given in Fig.21. Only the behavior of the minimum wavelength $\lambda = 25$ inches is shown since the other λ's show similar, but less critical trends.

From Figs.20 and 21, the transition between the undamped and the damped panel now becomes clear. It is seen that for low damping ratios, the divergence-type instability represented by Eq.34 is a very mild one, and the amplification A does not become significant until the air speed approaches that for the flutter-type instability represented by Eq.19. Correspondingly, the wave speed $(c + U)_R$ changes from zero to the value for the flutter-type instability given by Eq.20. For large damping ratios, the divergence-type instability does become significant. It is associated with very low speed travelling waves and hence would resemble divergence. The very interesting destabilizing effect of damping in the speed region between 101.5 mph and 105.5 mph is to be noted. Similar behavior has also been discussed by Landahl in Ref.4.

To conclude this section, it might be appropriate to give here basic formulas for the occurrence of flutter and divergence for these infinite panels on elastic foundations. Simple algebraic manipulation of Eqs.15, 16, 19, 21, 22, and 34 gives the dynamic pressure at flutter as

$$\frac{1}{2}\rho_\infty U_F^2 = \left(\frac{1+\mu}{2}\right)\left[\left(\frac{1.5+\mu}{.5+\mu}\right)^{1/4}+\left(\frac{.5+\mu}{1.5+\mu}\right)^{3/4}\right] K^{3/4} D^{1/4} \qquad (39)$$

and the dynamic pressure at divergence as

$$\tfrac{1}{2}\rho_\infty U_D^2 = .878\, K^{3/4} D^{1/4} \tag{40}$$

In the expression for $\frac{1}{2}\rho_\infty U_F^2$, the appropriate value of μ is found through consideration of Eqs.15, 21, and 22. As in many other types of flutter instability, the dynamic pressure at flutter becomes independent of mass density ratio for heavy panels and low density air ($\mu \to 0$).

3.3 Finite Panel in Incompressible Flow

It is of interest to analyze also the finite panel and compare results with those obtained for the infinite panel.

The differential equation to be solved is given by Eq.1 subject to the appropriate boundary conditions. For simplicity, the panel will be assumed pinned at both ends.* The aerodynamic pressure for air acting on the top side only,** can be expressed as

$$\Delta p = \frac{\rho_\infty}{\pi}\int_0^\ell \left(\frac{\partial^2 w}{\partial t^2} + U\frac{\partial^2 w}{\partial t \partial x}\right) \ln\left|\frac{x-\xi}{\ell}\right| d\xi + \frac{\rho_\infty}{\pi}\int_0^\ell \left(U\frac{\partial w}{\partial t} + U^2\frac{\partial w}{\partial x}\right)\frac{1}{x-\xi}\, d\xi \tag{41}$$

*The higher modes are of interest in this analysis, and for these, the different boundary conditions do not affect the modes and frequencies very much except in the immediate vicinity of the trailing edge.

**The pressure acting on the bottom side of the panel is again assumed constant at p_∞. The presence of still air on the bottom side of the panel is examined in Appendix A and is found to be small for the low μ's of interest here.

where w is the deflection of the panel. (See, for example, Ref.5). As the general solution of the integro-differential equation given by Eqs.1 and 41 is extremely difficult, a Galerkin-type solution will be used by assuming modal solutions of the form,

$$W(x,t) = \sum_{n=1}^{N} q_n(t) \sin \frac{n\pi x}{\ell} \tag{42}$$

These satisfy the pinned end boundary conditions at x = 0 and x = ℓ. Further, the aerodynamic pressure will be assumed to be that for an infinitely long wavy wall. This is a reasonable assumption except in the immediate vicinity of the leading and trailing edges, particularly for the higher modes (large n) of interest here. For such an infinite wavy wall of shape given by Eq.42, the aerodynamic pressure Δp of Eq.41 reduces simply to (see also for example Ref.6),

$$\Delta p = \sum_{n=1}^{N} \left\{ \left[-\frac{\rho_\infty \ell}{n\pi} \frac{d^2 q_n}{dt^2} + \rho_\infty U^2 \frac{n\pi}{\ell} q_n \right] \sin \frac{n\pi x}{\ell} - \left[2\rho_\infty U \frac{dq_n}{dt} \right] \cos \frac{n\pi x}{\ell} \right\} \tag{43}$$

Placing this expression together with Eq.42 into the basic panel Eq.1, and applying Galerkin's method, results in the series of ordinary differential equations

$$\left(m + \frac{\rho_\infty \ell}{n\pi}\right)\frac{d^2 q_n}{dt^2} + \left(D\frac{n^4\pi^4}{\ell^4} + K - \rho_\infty U^2 \frac{n\pi}{\ell}\right) q_n + \frac{8\rho_\infty U}{\pi} \sum^{n+r=\text{odd}} \left(\frac{n}{n^2-r^2}\right)\frac{dq_r}{dt} = 0 \tag{44}$$

$$n, r = 1, 2, \cdots N$$

The summation above is taken over all the r terms for which n + r is an odd integer. It is convenient to introduce the following nondimensional quantities.

$$\bar{t} = t\sqrt{\frac{D}{m\ell^4}} \qquad Q = \frac{\rho_\infty U^2 \ell^3}{D}$$

$$\tilde{\mu} = \frac{\rho_\infty \ell}{m\pi} \qquad \bar{K} = \frac{K\ell^4}{D} \tag{45}$$

With these definitions, the equations of motion, Eqs.44 become nondimensionalized to,

$$\left[1 + \frac{\tilde{\mu}}{n}\right]\frac{d^2 q_n}{d\bar{t}^2} + \left[n^4\pi^4 + \bar{K} - n\pi Q\right] q_n + \sqrt{\frac{Q\tilde{\mu}}{\pi}} \sum^{n+r=\text{odd}} \left(\frac{8n}{n^2-r^2}\right)\frac{dq_r}{d\bar{t}} = 0 \tag{46}$$

Solutions of the above equations are sought in the standard fashion in the form $e^{\bar{s}\,\bar{t}}$. In physical time, the solutions are given by $e^{s\,t}$ where

$$s = \bar{s}\sqrt{\frac{D}{m\ell^4}} \tag{47}$$

Consider now the coupling between the n and n + 1 modes. Upon introducing $e^{\underline{s}\,t}$ into Eq.46 one obtains,

$$\begin{bmatrix} \left\{\bar{s}^2\left[1+\frac{\tilde{\mu}}{n}\right]+\left[n^4\pi^4+\bar{K}-n\pi Q\right]\right\} & \left\{\bar{s}\sqrt{\frac{Q\tilde{\mu}}{\pi}}\,\frac{8n}{n^2-(n+1)^2}\right\} \\ \left\{\bar{s}\sqrt{\frac{Q\tilde{\mu}}{\pi}}\,\frac{8(n+1)}{(n+1)^2-n^2}\right\} & \left\{\bar{s}^2\left[1+\frac{\tilde{\mu}}{n+1}\right]+\left[(n+1)^4\pi^4+\bar{K}-(n+1)\pi Q\right]\right\} \end{bmatrix} \begin{Bmatrix} q_n \\ q_{n+1} \end{Bmatrix} = 0 \tag{48}$$

Setting the determinant of the above equations equal to zero yields the characteristic equation in $\bar{s}$

$$A_4\,\bar{s}^4 + A_2\,\bar{s}^2 + A_0 = 0 \tag{49}$$

where

$$\begin{aligned} A_4 &= \left(1+\frac{\tilde{\mu}}{n}\right)\left(1+\frac{\tilde{\mu}}{n+1}\right) \\ A_2 &= \left(1+\frac{\tilde{\mu}}{n}\right)\left[(n+1)^4\pi^4+\bar{K}-(n+1)\pi Q\right] \\ &\quad +\left(1+\frac{\tilde{\mu}}{n+1}\right)\left[n^4\pi^4+\bar{K}-n\pi Q\right]+\frac{64}{\pi}\,\frac{n(n+1)}{(2n+1)^2}\,\tilde{\mu}Q \\ A_0 &= \left[n^4\pi^4+\bar{K}-n\pi Q\right]\left[(n+1)^4\pi^4+\bar{K}-(n+1)\pi Q\right] \end{aligned} \tag{50}$$

The roots $\bar{s}$ of the characteristic equation, Eq.49, are examined as Q increases from zero. Real positive roots represent divergence conditions, while complex roots with positive real parts represent flutter instabilities.

First the static divergence behavior is examined. This occurs for $A_0 = 0$ which implies

$$Q = \frac{n^4\pi^4 + \bar{K}}{n\pi} \tag{51}$$

For the present panel, $\bar{K} = 1.46 \times 10^6$, and the quantity Q versus n is plotted in Fig.22. The minimum occurs for n = 8 and the corresponding value of Q, U, and wavelength at divergence are

$$\begin{aligned} Q_D &= 73{,}570 \\ U_D &= 101.5 \text{ mph} \\ \lambda &= 2\ell/n = 26 \text{ in} \end{aligned} \tag{52}$$

These values agree well with those obtained for the infinite panel and given by Eq.36.

Next, the complete dynamic behavior of the system is examined. Equation 49 can be solved to give the four roots $\bar{s}$ as

$$\bar{s} = \pm \sqrt{\frac{-A_2 \pm \sqrt{A_2^2 - 4A_4A_0}}{2A_4}} \tag{53}$$

Flutter (dynamic instability) will occur only if the inner radical $\sqrt{A_2^2 - 4A_4A_0}$ becomes an imaginary number, that is, if

$$A_2^2 - 4A_4A_0 < 0 \tag{54}$$

since only then will complex roots for $\bar{s}$ appear with positive real parts. Using the values given by Eqs.50, the above criterion for flutter, Eq.54 becomes

$$\left\{\left(1+\frac{\tilde{\mu}}{n}\right)\left[(n+1)^4\pi^4+\bar{K}-(n+1)\pi Q\right]-\left(1+\frac{\tilde{\mu}}{n+1}\right)\left[n^4\pi^4+\bar{K}-n\pi Q\right]\right\}^2$$

$$+\left\{\frac{64}{\pi}\frac{n(n+1)}{(2n+1)^2}\tilde{\mu}Q\right\}^2 < -\frac{128}{\pi}\frac{n(n+1)}{(2n+1)^2}\tilde{\mu}Q\left\{\left(1+\frac{\tilde{\mu}}{n}\right)\left[(n+1)^4\pi^4+\bar{K}-(n+1)\pi Q\right]\right.$$

$$\left.+\left(1+\frac{\tilde{\mu}}{n+1}\right)\left[n^4\pi^4+\bar{K}-n\pi Q\right]\right\} \qquad (55)$$

Since the left-hand side of the above criterion is always positive, it is obvious that flutter can only occur for negative values of $[n^4\pi^4 + \bar{K} - n\pi Q]$ or $[(n + 1)^4\pi^4 + \bar{K} - (n + 1)\pi Q]$; that is, only after the divergence speed has been exceeded. Hence, as in the infinite panel case, the finite panel in incompressible flow yields divergence below flutter. The above result has also been shown more generally for an infinite number of modes by Flax in Ref.6.

For the present panel, the four roots $\bar{s}$ associated with coupling between the 8^{th} and 9^{th} modes were computed using Eqs.53 and 50 for various values of Q. The four corresponding dimensioned roots s are shown in Fig.23 for various speeds. At low speeds, these roots represent two undamped steady sinusoidal oscillations. Then static divergence sets in for a very narrow band of speeds from 101.55 to 101.77 mph. Above this band, two undamped steady sinusoidal oscillations are again present. Finally, at speeds above 103.13 mph, flutter instability occurs.

The rate of growth associated with these instabilities is of interest. For this finite panel, the amplification

ratio $\tilde{A}$ is introduced which is defined now as the ratio of amplitudes during a time interval of $2\pi/21.3 = 0.295$ sec. This time interval represents the time for one oscillation at the flutter frequency and is chosen in an attempt to make the $\tilde{A}$ of the finite panel somewhat comparable to the A of the infinite panel. This amplification $\tilde{A}$ is then,

$$\tilde{A} = e^{.295\,(s)_{Real}} \tag{56}$$

and is shown plotted versus speed U in Fig.24. Again it is seen that the divergence instability is a very mild one compared to the strong instability associated with the flutter behavior. This fact together with the narrow speed band associated with this divergence seems to indicate that flutter will be the dominant instability, at least for this simplified two-mode example.

The steady oscillations occurring both below and above the divergence speed bands were investigated in more detail. Figure 25 presents a plot of the frequencies ω versus air speed as obtained from the basic roots s of Fig.2 The mode shapes associated with these frequencies can be obtained from Eqs.48. Using the first of these equations, it can be shown that for a harmonic oscillation of the form,

$$q_8(t) = \cos \omega t \tag{57}$$

The associated mode $q_9(t)$ is given by

$$q_9(t) = f_2 \sin \omega t \tag{58}$$

where,

$$f_2 = \frac{(2n+1)}{8n}\sqrt{\frac{\pi}{Q\tilde{\mu}}}\left\{\frac{(n^4\pi^4+\bar{K}-n\pi Q)}{|\bar{s}|} - |\bar{s}|\left(1+\frac{\tilde{\mu}}{n}\right)\right\} \qquad (59)$$

and the frequency ω is the absolute magnitude of a pure imaginary pair of roots s such as occur in Fig.23. The nondimensional root $\bar{s}$ appearing above is related to s through Eq.47. Then, the deflection shape for these steady oscillations is given by,

$$W(x,t) = \cos\omega t \sin\frac{n\pi x}{\ell} + f_2 \sin\omega t \sin\frac{(n+1)\pi x}{\ell} \qquad (60)$$

Thus, the two standing wave mode shapes sin $n\pi x/\ell$ and sin $(n+1)\pi x/\ell$ are coupled together 90 degrees out of phase by the aerodynamic damping forces. This is true for all the steady oscillations occurring below or above the divergence speed band.

The mode coupling factor f_2 plays an interesting role in Eq.60. Values of this factor $f_2 = 0$ and $f_2 = \infty$ represent pure standing waves in the sin $n\pi x/\ell$ and sin $(n+1)\pi x/\ell$ modes, respectively, while values of $f_2 = +1$ and $f_2 = -1$ represent approximately travelling waves in the upstream and downstream directions, respectively. This latter fact can be seen by rewriting the deflection shape Eq.60 equivalently as,

$$W(x,t) = \cos\omega t\left[\sin(n+\tfrac{1}{2})\frac{\pi x}{\ell}\cos\frac{\pi x}{2\ell} - \cos(n+\tfrac{1}{2})\frac{\pi x}{\ell}\sin\frac{\pi x}{2\ell}\right]$$
$$+ f_2 \sin\omega t\left[\sin(n+\tfrac{1}{2})\frac{\pi x}{\ell}\cos\frac{\pi x}{2\ell} + \cos(n+\tfrac{1}{2})\frac{\pi x}{\ell}\sin\frac{\pi x}{2\ell}\right] \qquad (61)$$

Near the center portion of a long panel,

$$\cos\frac{\pi x}{2\ell} \approx \sin\frac{\pi x}{2\ell} \approx .7071 \qquad (62)$$

This approximation is particularly good for long panels where n is large. Then, Eq.61 reduces to

$$\begin{aligned} W(x,t) &\approx \sin\left[\omega t + (n+\tfrac{1}{2})\frac{\pi x}{\ell} - 45^\circ\right] \qquad \text{For } f_1 = +1 \\ W(x,t) &\approx \sin\left[\omega t - (n+\tfrac{1}{2})\frac{\pi x}{\ell} + 45^\circ\right] \qquad \text{For } f_1 = -1 \end{aligned} \qquad (63)$$

These are readily identified as waves travelling to the left (upstream) and to the right (downstream), respectively.

A plot of the factor f_2 versus air speed for this panel is given in Fig.26. The behavior of these steady oscillations then becomes clear. At very low speeds, they represent more or less pure standing waves. As the speed increases, they rapidly develop into two travelling waves, the lower frequency branch L moving upstream, the higher one H moving downsteam. At the divergence speed, the lower frequency branch L, drops sharply to zero indicating a divergence in the lower mode 8 again. At the upper divergence speed, the divergence occurs in the higher mode 9. Above the narrow divergence speed gap, the lower frequency branch LL reappears and rapidly becomes a travelling wave now moving downstream. At the flutter speed, the two travelling waves coalesce and give rise to unstable oscillations. A sketch of the oscillations at flutter is given in Fig.27. The travelling wave character of these oscillations is clearly apparent.

The characteristics at flutter are calculated from this two degrees of freedom analysis as,

$$\begin{aligned} &\text{Flutter speed } U_F = 103.1 \text{ mph} \\ &\text{Flutter frequency } \omega_F = 21.3 \text{ rad/sec} = 3.4 \text{ cps} \\ &\text{Wavelength } \lambda = 2\ell/(n + \tfrac{1}{2}) = 24.5 \text{ in} \\ &\text{Wave speed } c + U = \omega\lambda/2\pi = 6.9 \text{ ft/sec} \end{aligned} \tag{65}$$

These are to be compared with the corresponding values for the infinite panel given by Eq.23. The flutter speeds are similar; however, the flutter frequency and wave speed are somewhat lower here.

The general behavior of the two degrees of freedom finite panel analysis closely resembles the infinite panel analysis described in Section 3.2. The divergence speed, the mild character of divergence, the undamped travelling waves moving in opposite directions below the divergence speed and in the same direction above the divergence speed (compare with Fig.17), and finally their merging together to form a strong flutter, are all present here. The characteristics at divergence and flutter are also quite similar. Presumably, the presence of more modes and some additional internal damping would bring the results of the finite and infinite panel analyses even more closely in line with one another, particularly for instabilities occurring at high values of n. Thus, a smooth transition between the finite panel, standing wave analysis at low values of n to the infinite panel, travelling wave analysis at high values of n is observed.

To conclude this section, it might be appropriate to give here a simple criterion for these finite panels on elastic foundations. Using Eq.51, the onset of divergence can be defined by the nondimensional parameter Q which is a function only of $\bar{K}$. This is shown plotted in Fig.28. For

values of $\bar{K}$ greater than 2000, the curve shown there can be approximated by

$$Q \approx 1.755\ \bar{K}^{3/4} \tag{66}$$

$$n \approx .242\ \bar{K}^{1/4} \quad \text{(nearest integer)} \tag{67}$$

The criterion Eq.66 reduces identically to that given by Eq.40 for the infinite panel. As discussed in Sections 3.2 and 3.3, these divergence criterions represent only a lower bound on the occurrence of instability. The actual instability is more apt to be the stronger flutter-type instability which occurs somewhat above the divergence speed quoted here.

4. COMPARISON OF EXPERIMENT AND THEORY

The experimental test results obtained for this panel were described in detail in Section 2.5, and were summarized in Section 2.5f. These results indicated definite flutter with the following approximate characteristics,

$$\begin{aligned} U_F &\approx 95 \text{ mph} \\ \lambda &\approx 27 \text{ inches} \\ c + U &\approx 35 \text{ ft/sec} \\ \omega &\approx 14.4 \text{ cps} \end{aligned} \tag{68}$$

The waves generally appeared to be travelling downstream, although there seemed to be some standing wave component present near the center of the panel. Below the occurrence of flutter, the panel assumed a small static sinusoidal deflection shape of about two-foot wavelength over the rear half of the panel.

The theoretical results for this panel were described in detail in Section 3, and showed essentially the same behavior from both the infinite panel and finite panel point of view. Using the infinite panel analysis, these results indicated a strong travelling wave-type flutter developing with the following characteristics,

$$U_F = 105.5 \text{ mph}$$

$$\lambda = 25 \text{ inches}$$

$$c + U = 11.4 \text{ ft/sec}$$

$$\omega = 5.5 \text{ cps}$$

In addition, a much milder instability of static divergence type was also shown to exist for this lightly damped panel

at the slightly lower speed of 101.5 mph and with essentially the same $\lambda = 25$ inches.

Comparing these experimental and theoretical results, it is seen that there is good agreement in the flutter speed and wavelength, but rather poor agreement in the wave speed and frequency at flutter. Below the flutter speed, the observed small static deflections agree well in wavelength with those of theory.

The poor agreement found here in wave speed and frequency at flutter is typical of other aeroelastic phenomena in which the flutter frequency is less accurately predicted than the flutter speed. Looking at the variation of wave speed $c + U$ with air speed given in Fig.17 or at the variation in frequency ω with air speed given in Fig.25, it is seen that very small changes in air speed have great effects on the wave speed and frequency in the vicinity of the flutter speed. The prediction of $c + U$ and ω seems here generally more difficult than that of air speed.

Some specific factors which may have contributed to the poor agreement in wave speed and frequency are given below.

a) The static depression at the leading edge. This shortened the effective length of the panel and may have introduced midplane tension and structural nonlinearities into the panel behavior. It is felt that this effect was the primary reason for the scatter in the experimental results at high, medium, and low angles of attack. Also, this probably contributed to the appearance of the large static deflections of Runs 114 through 121. More care should be taken to maintaining uniform pressure and velocity distributions over the panel surface by better wall contouring and venting.

b) The cavity effect of the still air on the bottom side of the panel. The effect of still air of infinite depth on the bottom side of the panel was investigated in Appendix A and found to be negligible for this panel. However, it may be that for the finite depth of about 2 1/2 inches here, the cavity resonance effect may be more appreciable. Also, the large amplitudes of the flutter deflections may have had an influence here.

c) Buffeting at the trailing edge. There may have been some forcing oscillations caused by rough flow at the trailing edge, particularly when the edge was free. The somewhat similar experimental results obtained for the case of free and pinned edges seem to minimize this source of disturbance.

d) Boundary-layer effects. The effects of a boundary layer in influencing panel flutter behavior have recently been suggested. Some investigations have been carried out by Miles in Ref.7, and more recently, Landahl in Ref.4, studied the stability of a boundary layer in the presence of a flexible wall. It is believed this specific panel lies outside the range of any such significant effects.

5. CONCLUSIONS

The present report has investigated the subsonic flutter of panels on continuous elastic foundations. Interesting phenomena have been observed both experimentally and theoretically.

Experimentally, definite flutter was observed for a specific panel in this subsonic flow. The flutter was of a travelling-wave type, although there seemed to be some standing wave component present near the center of the panel. Below the occurrence of flutter, the panel assumed a small static sinusoidal deflection shape over the rear half of the panel.

Theoretically, it has been shown that a finite panel analysis gives essentially the same behavior as the infinite panel analysis for high values of n (or ℓ/λ). Thus, a smooth transition is demonstrated between the finite panel, standing wave analysis at low values of n to the infinite panel, travelling wave analysis at high values of n. It has also been demonstrated that although a mild static-divergence-type instability may exist for these panels, the dominant instability will be a travelling wave, flutter-type instability. The role of additional internal damping was also investigated for these panels, and was shown to have an interesting destabilizing effect in the region between the divergence speed and the flutter speed.

Comparison of the experimental results with theory showed good agreement in the prediction of a travelling wave-type flutter, the flutter speed, and the wavelength. However, there was rather poor agreement in the

prediction of the wave speed and frequency at flutter. Outside of the general difficulty of predicting the wave speed and frequency as accurately as the flutter speed, this discrepancy was attributed possibly to limitations in the experiment arising from a static depression at the leading edge of the panel, the cavity effect of the still air on the bottom side of the panel, buffeting at the trailing edge, and boundary-layer effects.

Much further work remains to be done on this general problem area to understand it more fully. More careful experiments, better agreement in wave speeds and frequencies, experimental verification of the interesting relationship of divergence, flutter, and internal damping, the effects of still-air cavities, the effects of boundary layers, all need yet to be done. The related problem of subsonic flutter of panels without elastic foundations is also of considerable interest. Some interesting work has been done by Greenspon and Goldman in Ref.8 and again the existence of experimental subsonic flutter was revealed. These subsonic investigations should be of interest in the problems of hydroelastic panel flutter, axially-symmetric cylinder flutter at low speeds, and panel flutter of inflatable structures at low speeds.

The extension of this work to the supersonic flutter of panels on continuous elastic foundations would also be of considerable interest. Here again, Miles' infinite panel theory of Ref.1 can be used as a reference, and the effects of a finite panel, internal damping, etc. can again be investigated and compared with experiment.

APPENDIX A

INFLUENCE OF STILL AIR ON BOTTOM SIDE OF PANEL

In the theory developed in Section 3, the pressure acting on the bottom side of the panel was assumed constant at the value p_∞. It is of interest to investigate the additional pressure caused by the presence of still air on this bottom side.

a) Infinite Panel

The pressure on the bottom surface of a sinusoidal wave travelling with wave speed $\bar{c}$ through still air has been shown by Miles in Ref.1 to be

$$\Delta p(\bar{x},t) = \rho_\infty \frac{2\pi}{\lambda} \bar{c}^2 w_o \, e^{i\frac{2\pi}{\lambda}(\bar{c}t - \bar{x})} \qquad \text{(A-1)}$$

In the above, $\bar{x}$ represents the distance relative to the panel and $\bar{c}$ represents the wave speed relative to the panel. To convert the above results to the axis system used by Miles in his analysis and repeated again in Section 3.2, one notes that

$$x = \bar{x} - Ut \qquad \text{(A-2)}$$

$$c = \bar{c} - U \qquad \text{(A-3)}$$

where x and c refer to a fixed axis system, and the plate itself moves with velocity U in the negative x direction. Placing Eqs.A-2 and A-3 into Eq.A-1 gives the additional pressure from the bottom side of the panel as

$$\Delta p(x,t) = \rho_\infty \frac{2\pi}{\lambda} (c+U)^2 w_o \, e^{i\frac{2\pi}{\lambda}(ct - x)} \qquad \text{(A-4)}$$

The above pressure is added to that for the top side of the panel given by Eq.11, and then substituted into the moving panel equation, Eq.9. Upon nondimensionalization as before, one now obtains the equation

$$(\zeta + 1)^2 - \zeta_o^2 + \mu(2\zeta^2 + 2\zeta + 1) = 0 \qquad \text{(A-5)}$$

in place of the previous Eq.12.

Solving Eq.A-5 explicitly for ζ, one obtains the following expressions for the wave speed relative to still air, c,

$$c = \frac{1}{1+2\mu}\left\{-(1+\mu)U \pm \sqrt{(1+2\mu)c_o^2 - \mu(1+\mu)U^2}\right\} \qquad \text{(A-6)}$$

and for the wave speed relative to the panel $c + U = \bar{c}$,

$$c + U = \frac{1}{1+2\mu}\left\{\mu U \pm \sqrt{(1+2\mu)c_o^2 - \mu(1+\mu)U^2}\right\} \qquad \text{(A-7)}$$

These expressions are to be compared with the previous expressions Eqs.17 and 18, which neglected the air pressure variation on the bottom side of the panel.

It is readily seen from the above, that negative imaginary values of c, hence instability, occur now for

$$\frac{U}{c_o} > \sqrt{\frac{1+2\mu}{\mu(1+\mu)}} \qquad \text{(A-8)}$$

This criterion is indicated in Fig.14 by the dashed lines. For values of $\mu < 0.3$, this new flutter criterion is the same as the previous one given by Eq.19. At the higher

values of μ, it approaches 1.414 times the divergence criterion. The corresponding wave speed relative to the panel at flutter is

$$c + U = \frac{\mu U}{1 + 2\mu} \tag{A-9}$$

For the present panel, the characteristics at flutter with still air on the bottom side are calculated as

$$\begin{aligned} U_F &= 105.3 \text{ mph} \\ \lambda &= 25 \text{ in} \\ c + U &= 10.5 \text{ ft/sec} \\ \omega &= \frac{2\pi}{\lambda}(c + U) = 31.7 \text{ rad/sec} = 5.1 \text{ cps} \\ \mu &= 0.079 \end{aligned} \tag{A-10}$$

Comparing these with the corresponding ones Eq.23, it is seen that there is a negligible change in flutter speed, and only a slight modification to the wave speed and frequency.

The divergence characteristics remain unaltered by the presence of this still air. Also, the general character of transition between the divergence speed and flutter speed is identical for the low μ of this panel. At the higher μ's, some modification might be present.

The theory of this appendix would be important for panels with high μ's such as might result for very light panels, for very soft spring foundations K (hence large λ_{min}), or for heavy fluid media such as water, where the fluid was present both on the top and bottom side of the panel. For cases where water is present only on the top side and air is on the bottom side, the theory of Section

3.2 would be more applicable.

The analysis presented here considered the still fluid to be large in depth. The effect of a small depth cavity on the pressure distribution was not investigated here. Conceivably, it could give a greater influence on the flutter characteristics.

b) Finite Panel

The additional pressure from the vibration of the bottom side of the panel in still air is

$$\Delta p = \frac{\rho_\infty}{\pi} \int_0^{\ell} \frac{\partial^2 w}{\partial t^2} \ln \left| \frac{x-\xi}{\ell} \right| d\xi \qquad \text{(A-11)}$$

This represents purely an additional virtual mass term. Carrying through the analysis as in Section 3.3 will result in the set of nondimensional differential equations

$$\left[1 + 2\frac{\tilde{\mu}}{n}\right] \frac{d^2 q_n}{d\bar{t}^2} + \left[n^4\pi^4 + \bar{K} - n\pi Q\right] q_n + \sqrt{\frac{Q\tilde{\mu}}{\pi}} \sum^{n+r=odd} \left(\frac{8n}{n^2-r^2}\right) \frac{dq_r}{d\bar{t}} = 0 \qquad \text{(A-12)}$$

The only difference between the above equation and the previous Eq.46 is the presence of a factor 2 in the $d^2q_n/d\bar{t}^2$ term, representing a doubling of the virtual mass. The characteristic equation for the coupling of the n^{th} and $n+1^{th}$ modes is given again by Eq.49, but now the coefficients A_4 and A_2 would reflect this doubled virtual mass.

For the present panel, the four roots $\bar{s}$ were again computed. The divergence speed gap is unaffected and remains

between 101.55 and 101.77 mph as before. The characteristics at flutter are now computed as

$$\begin{aligned} &\text{Flutter speed } U_F = 103.07 \text{ mph} \\ &\text{Flutter frequency } \omega_F = 19.8 \text{ rad/sec} = 3.2 \text{ cps} \\ &\text{Wavelength } \lambda = 24.5 \text{ in} \\ &\text{Wave speed } c + U = \omega\lambda/2\pi = 6.5 \text{ ft/sec} \end{aligned} \tag{A-13}$$

Comparing these with the corresponding Eq.65, it is again seen that there is a negligible change in flutter speed and only a slight modification to the flutter frequency.

REFERENCES

1. Miles, J.W. On the Aerodynamic Instability of Thin Panels. Journal of the Aeronautical Sciences, Vol.23, No.8, pp.771-791, August 1956.

2. Dowell, E. The Dynamic Instability of Panels on Elastic Supports in a Supersonic Flow. Masters Thesis, Department of Aeronautics and Astronautics, M.I.T., February 1961.

3. Leonard, R.W., and Hedgepeth, John M. On Panel Flutter and Divergence of Infinitely Long Unstiffened and Ring-Stiffened Thin-Walled Circular Cylinders. NACA TR 1302, Langley Aeronautical Laboratory, Langley Field, Va., 1957.

4. Landahl, M.T. On the Stability of an Incompressible Laminar Boundary Layer over a Flexible Surface. To be published shortly in the Journal of Fluid Mechanics.

5. Bisplinghoff, R.L., Ashley, H., and Halfman, R.L. Aeroelasticity. Addison-Wesley Publishing Company, Inc., Cambridge, Mass., 1955.

6. Flax, A.H. Aero- and Hydro-Elasticity, article in Structural Mechanics, Proceedings of the First Symposium on Naval Structural Mechanics, Stanford University, California, August 11-14, 1958. Pergamon Press, New York, 1960.

7. Miles, J.W. On Panel Flutter in the Presence of a Boundary Layer. Journal of the Aerospace Sciences, Vol.26, No.2, pp.81-93, February 1959.

8. Greenspon, J.E., and Goldman, R.L. Flutter of Thin Panels at Subsonic and Supersonic Speeds. OSR Technical Report No.57-65, ASTIA No.136, 560, Dynamics Research Staff, The Martin Company, July 1957.

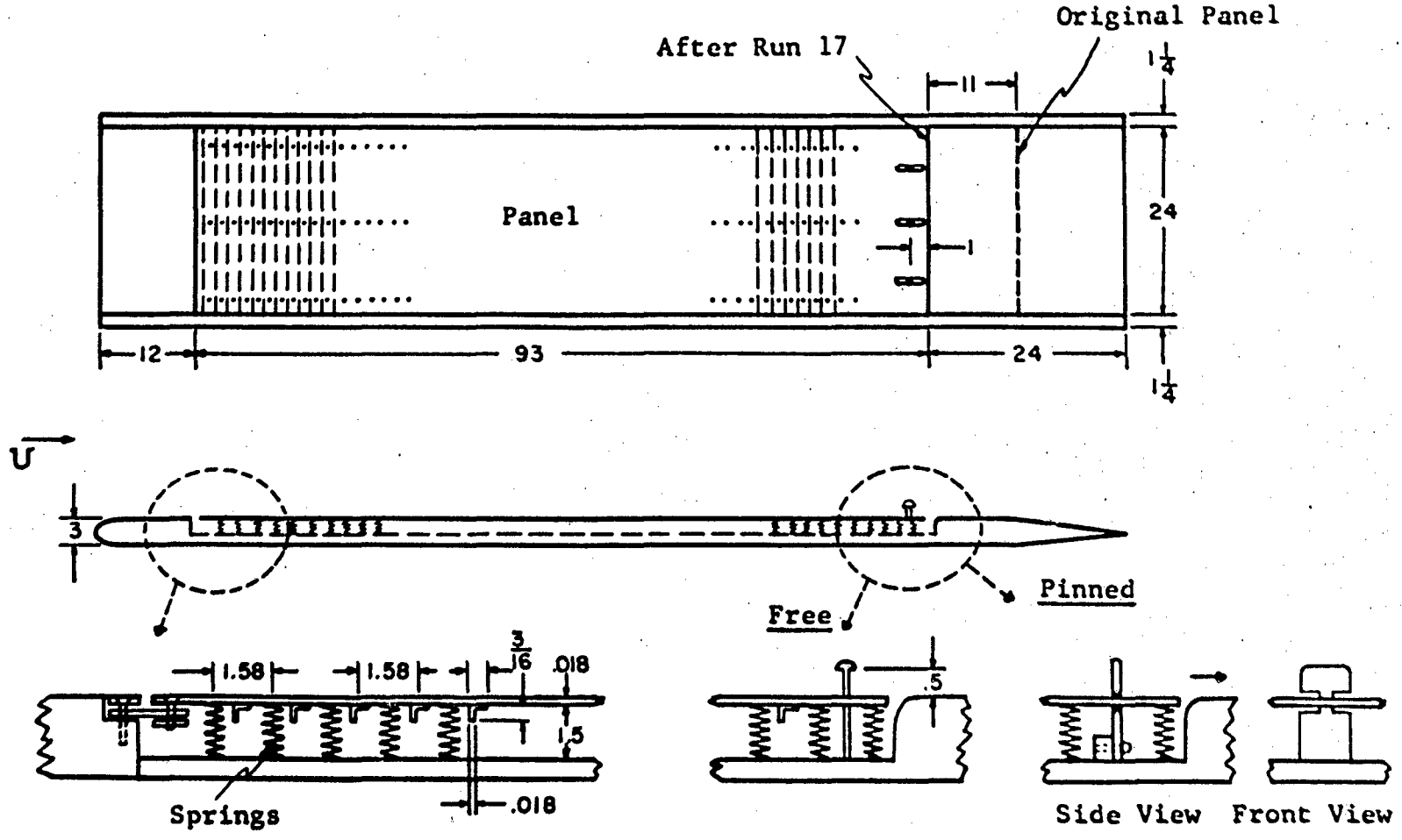

Fig.1 Panel Test Model and Wooden Frame

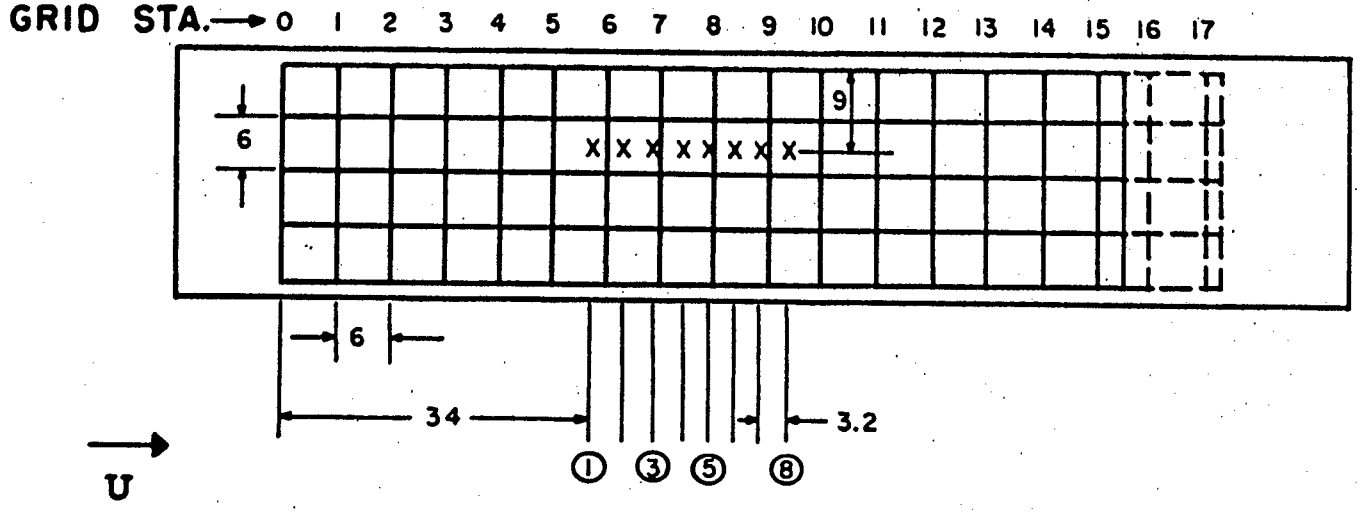

Fig.2 Location of Grid and Strain Gages

Fig.3 Spring Characteristics

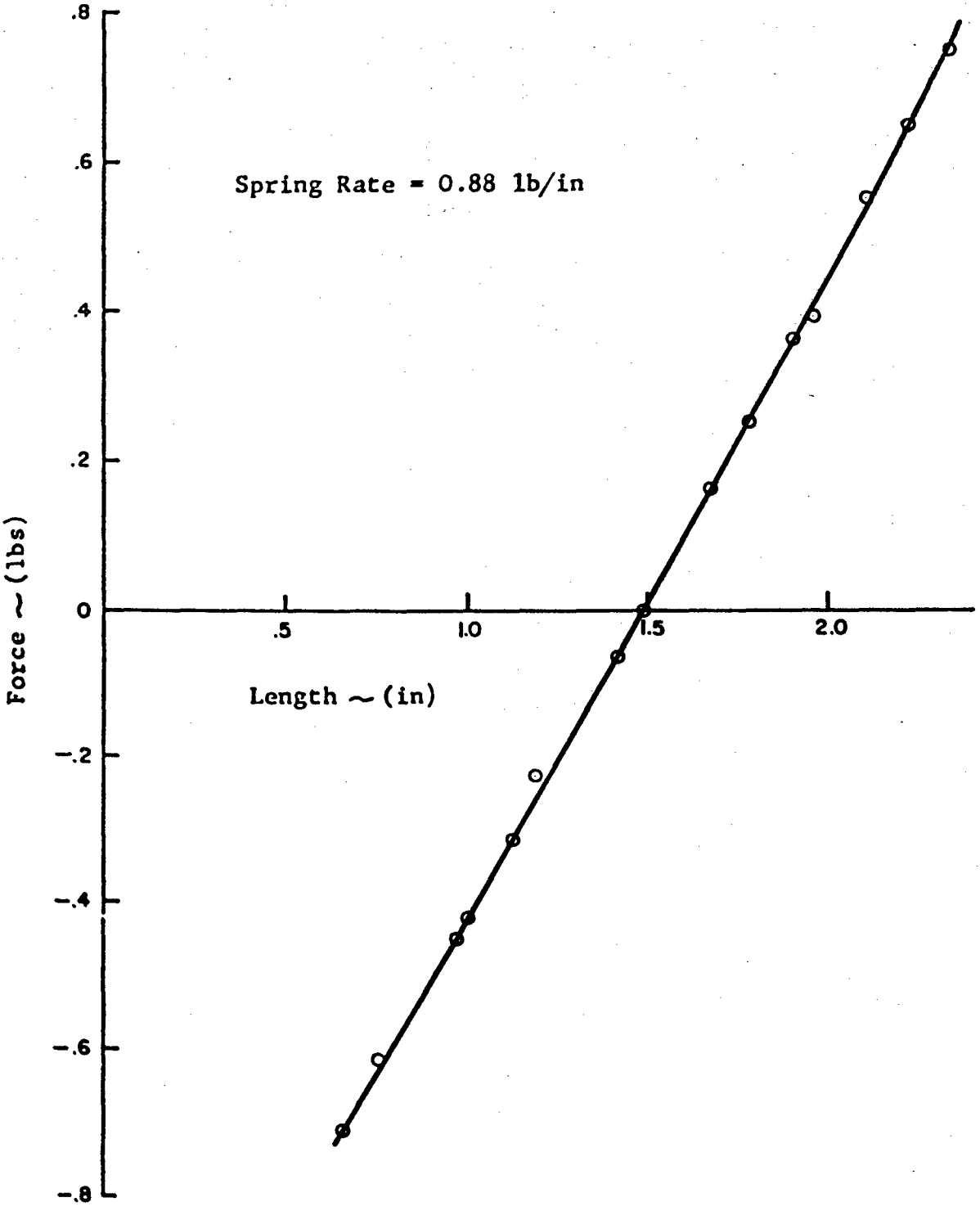

Fig.4 Vibration Modes of Panel

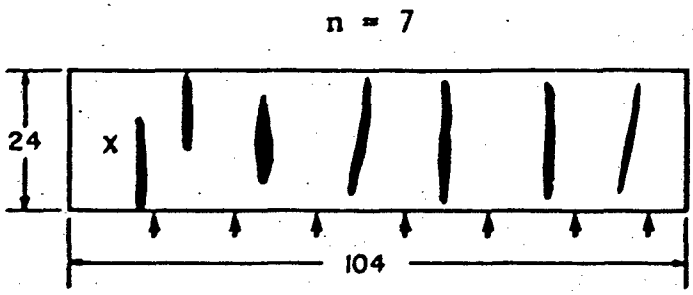

$\omega_{exp.}$ = 16.7 c.p.s

$\omega_{theo.}$ = 19.0 (vacuum)
17.4 (still air)

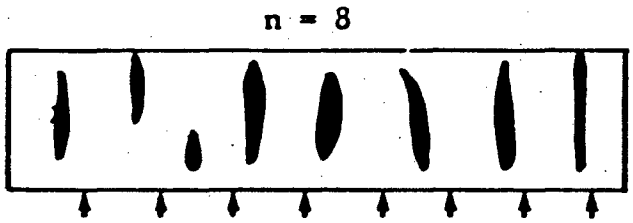

$\omega_{exp.}$ = 17.5 c.p.s

$\omega_{theo.}$ = 20.0 (vacuum)
18.5 (still air)

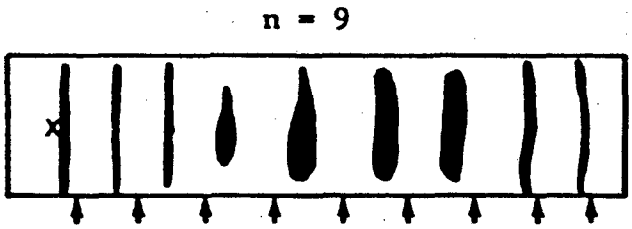

$\omega_{exp.}$ = 19.0 c.p.s

$\omega_{theo.}$ = 21.3 (vacuum)
19.9 (still air)

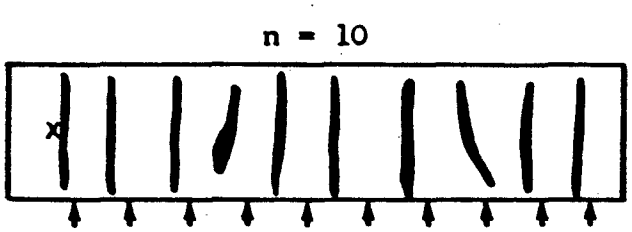

$\omega_{exp.}$ = 21.0 c.p.s

$\omega_{theo.}$ = 23.0 (vacuum)
21.6 (still air)

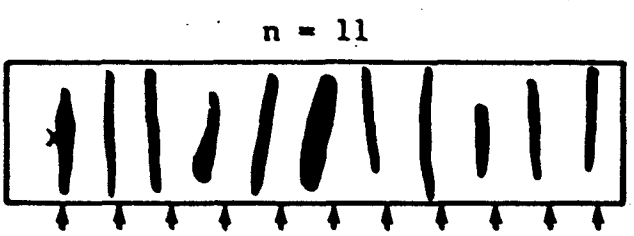

$\omega_{exp.}$ = 22.8 c.p.s.

$\omega_{theo.}$ = 25.2 (vacuum)
23.8 (still air)

Experimental node lines ———

Theoretical node lines indicated by arrows, ↓

Fig.5 Mounting in Tunnel

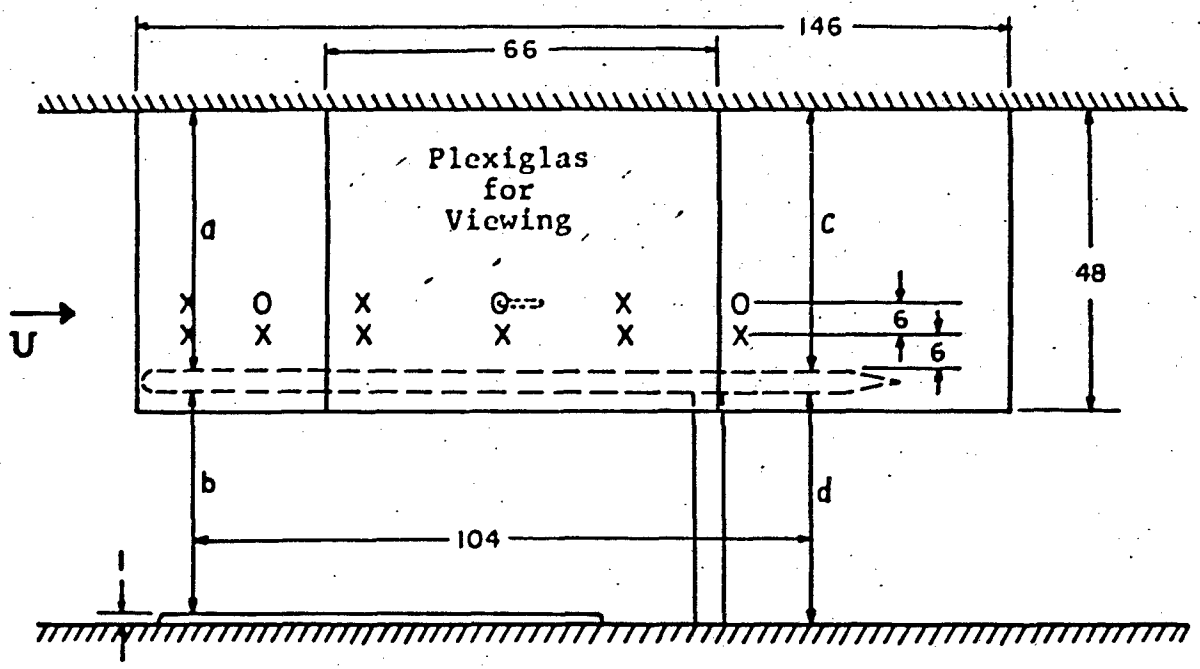

Dimension	High α	Med. α	Low α
a	41.8	42.4	42.9
b	38.1	37.5	37.0
c	44.7	43.9	42.7
d	36.7	37.5	38.7

O - Orig.pitot-static tubes

X - Add'l " " "

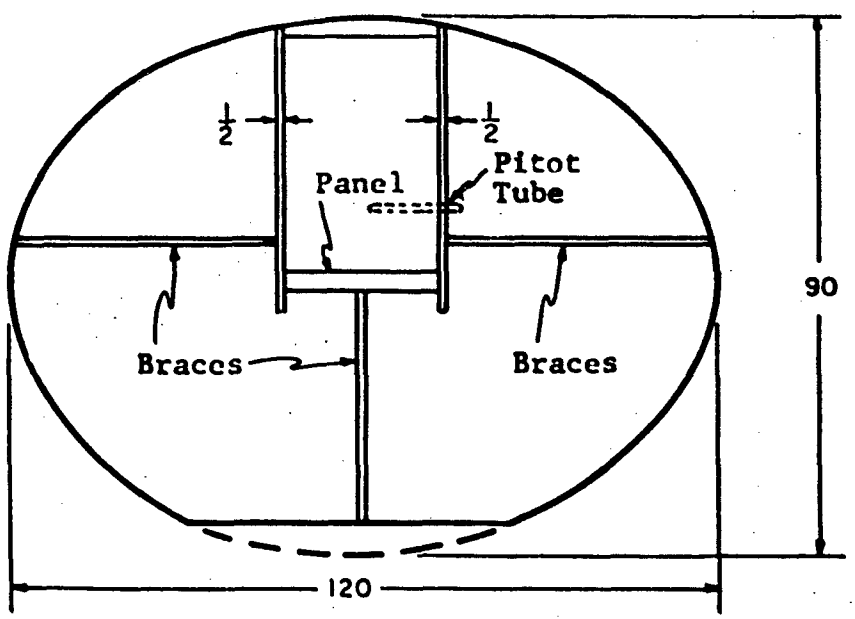

Fig. 6 Flutter Test Log

Runs	Angle of Attack	T.E. Condition	Panel Length	Comments*
Free End Panels				
1-17	Low α	Free	104"	Flutter @ 8.20(12),8.00(17)
18-21	Low α	"	93"	No Flutter to 5.90(21)
22-33	Med α	"	93"	Flutter @ 5.70(28),5.60(33)
34-40	High α	"	93"	Flutter @ 4.65(37) to 5.00(40)
41-51	Med α	"	93"	Flutter @ 5.24(44),5.20(48), 5.11(50)
Pinned End Panels				
52-79	Med α	Pinned	92"	Flutter @ 6.8 (77)
80-91	High α	"	92"	Flutter @ 5.0(86) to 5.5(91)
92-99	Med α	"	92"	Flutter @ 6.8(98)
Pressure & Velocity Surveys				
100-104	Med α	Pinned	92"	Flutter @ 6.0(104)
105-110	High α	"	92"	Flutter @ 5.0(109)
111-121	Low α	"	92"	No Flutter to 8.0(121), Strong Divergence
122-125	Med α	"	92"	Mild Flutter @ 5.5(124)
126**	Med α	Free	93"	Flutter @ 4.2(126)**

*First number refers to tunnel setting.
Second, in parentheses, refers to Run No.
**Discard this Run. Springs were loose @ T.E.

Fig.7 Static Pressure Survey

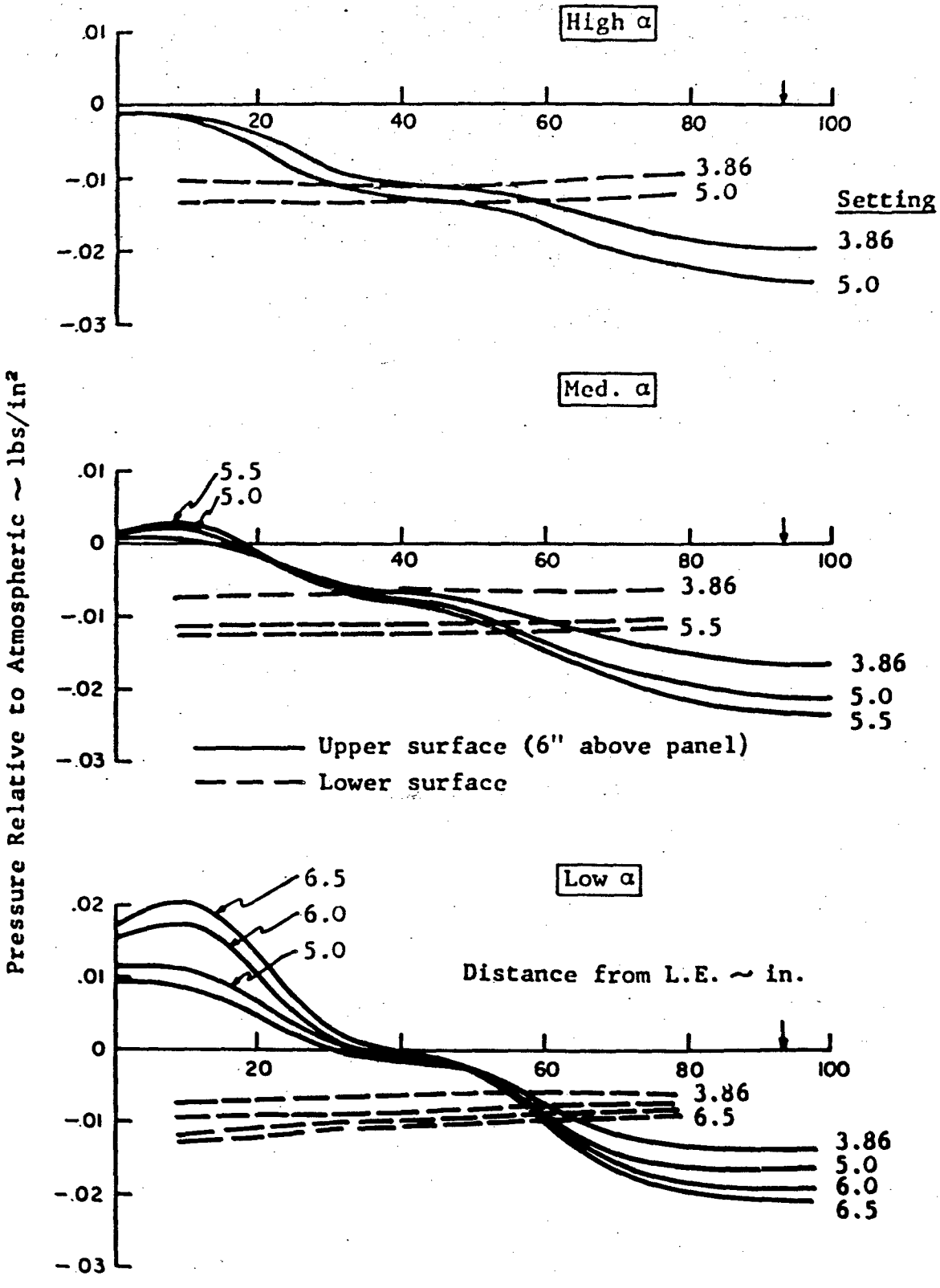

Fig.8 Velocity Survey

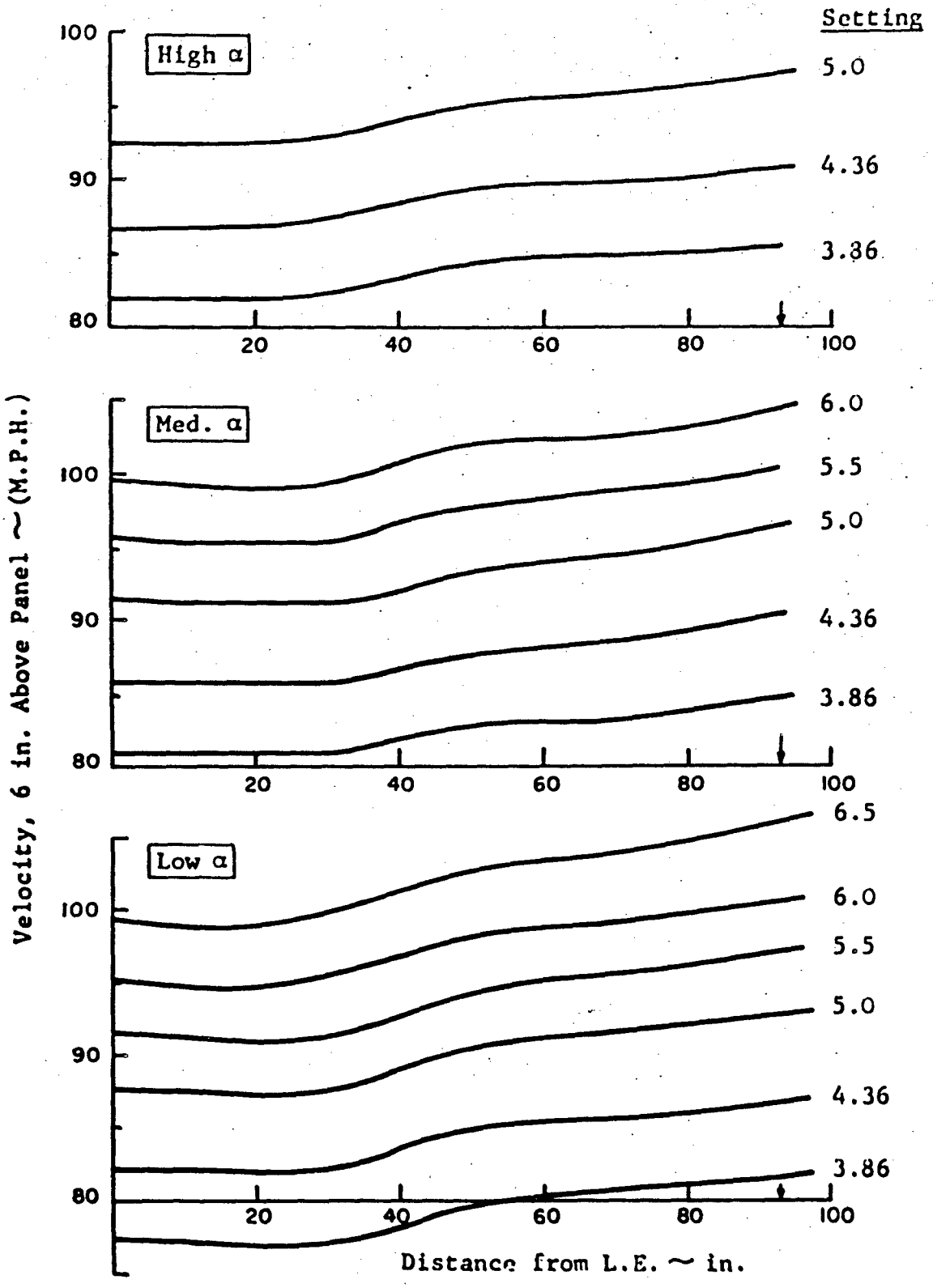

Fig.9 Panel Static Deflections

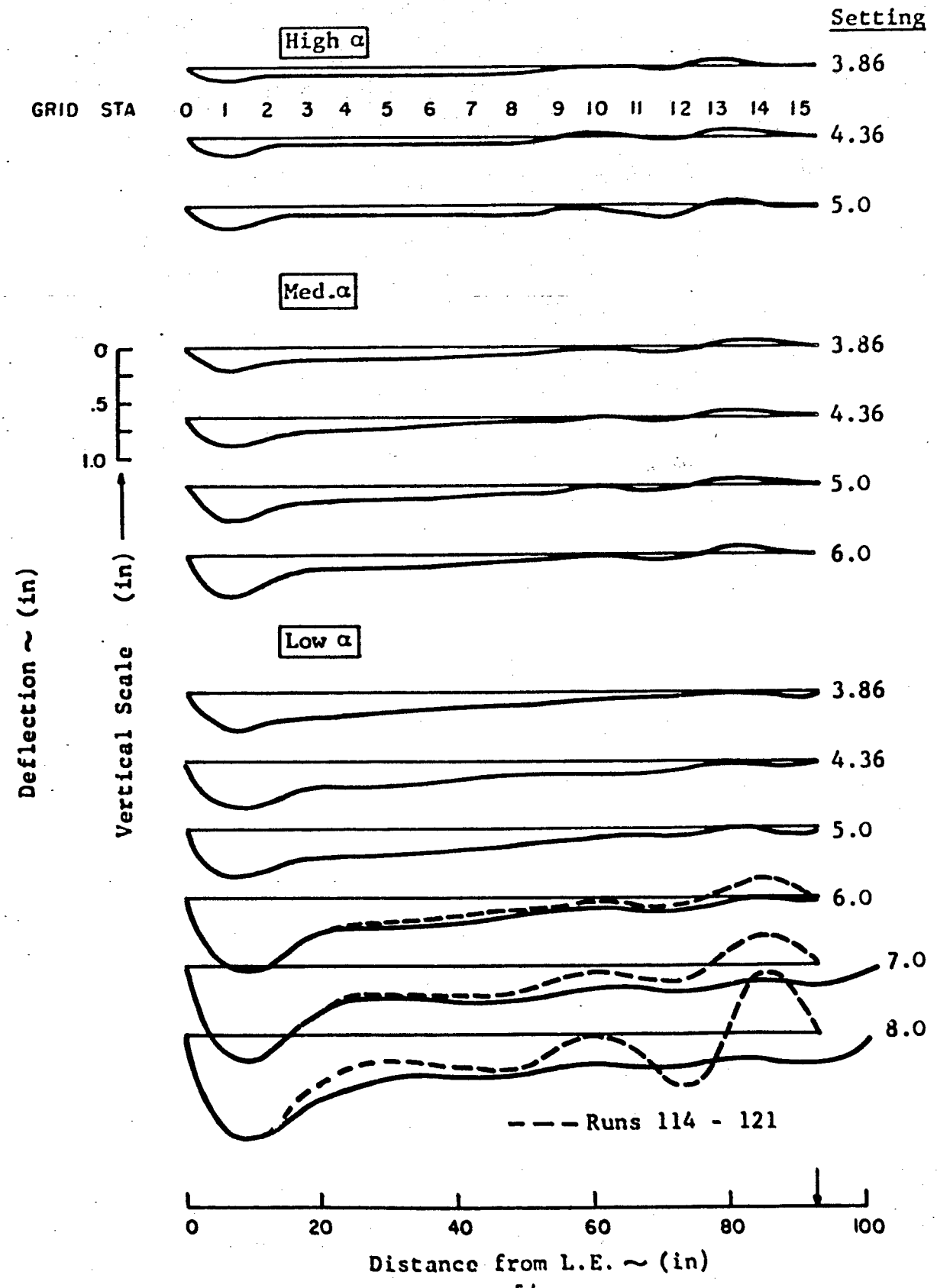

Fig. 10 Summary of Flutter Observations

High α

Free End: 4.65-5.0 (Runs 34-41) ⟶ 93-96 M.P.H.

Pinned End: 5.0 - 5.5 (Runs 86-91) ⟶ 96-100 M.P.H.
5.0(Run 109) ⟶ 96 M.P.H.

$V_F \approx$ 95 M.P.H.

$\omega_F \approx$ 14.4 c.p.s.

Med α

Free End: 5.7, 5.6 (Runs 28,33) ⟶ 101, 100 M.P.H.
5.24, 5.2, 5.11 (Runs 44, 48, 50) ⟶ 97, 97, 96 M.P.H.

Pinned End: 6.8, 6.8 (Runs 77, 98) ⟶ 108, 108 M.P.H.
6.0, 5.5 (Runs 104, 124) ⟶ 103, 99 M.P.H.

$V_F \approx$ 100 M.P.H.

$\omega_F \approx$ 13.9 c.p.s.

Low α

Free End: 8.2, 8.0 (Run 12, 17) ⟶ 117, 116 M.P.H.

Pinned End: Strong Divergence @ 8.0(121) ⟶ 116 M.P.H.

$V_F \approx$ 116 M.P.H. (Also Strong Divergence)

$\omega_F \approx$ 12.2 c.p.s.

Fig. 11 Film Log

Film	α	End	Setting	Run	Oscill.	Comments
1	High	Free	4.65	37	1286	Steady Flutter
2		"	4.8	38	1287	Steady Fl. (up front)
3		"	4.6-5.0	40	1288	Starting in Fl.
4		Pinned	4.6	82	1318	Slight Movements
5		"	4.9	85	-	More Movements
6		"	5.0	86	1319	Steady Fl.
7		"	5.5	91	1327	Steady Fl. (up front)
8		Pinned	5.2	110	1374	Steady Fl. (sweep front)
9	Med.	Free	5.7	28	1276	Starting in Fl.
10		"	5.6	33	1282	Starting in Fl.
11		Free	5.24	44	1290	Steady Fl.
12		"	5.24	44	1290	Steady Fl. (sweep front)
13		"	5.28	46	1291	Steady Fl.
14		"	5.20	48	1292	Steady Fl. (sweep front)
15		"	5.11	50	1293	Steady Fl. - Beats
16		"	4.6-5.1	51	1294	Starting in Fl.-Beats
17		Pinned	6.8	77	1306	Starting in Fl.
18		"	6.8	79	1307	Starting in Fl.
19		Pinned	6.0	104	1364	Steady Fl.
20		"	6.0	104	1365	Steady Fl. (up front)
21		Free	4.2	126	-	Steady Fl. (Discard this Run Springs loose @ T.E.)
22	Low	Pinned	8.0	121	-	Divergence

Fig.12a Movie Film

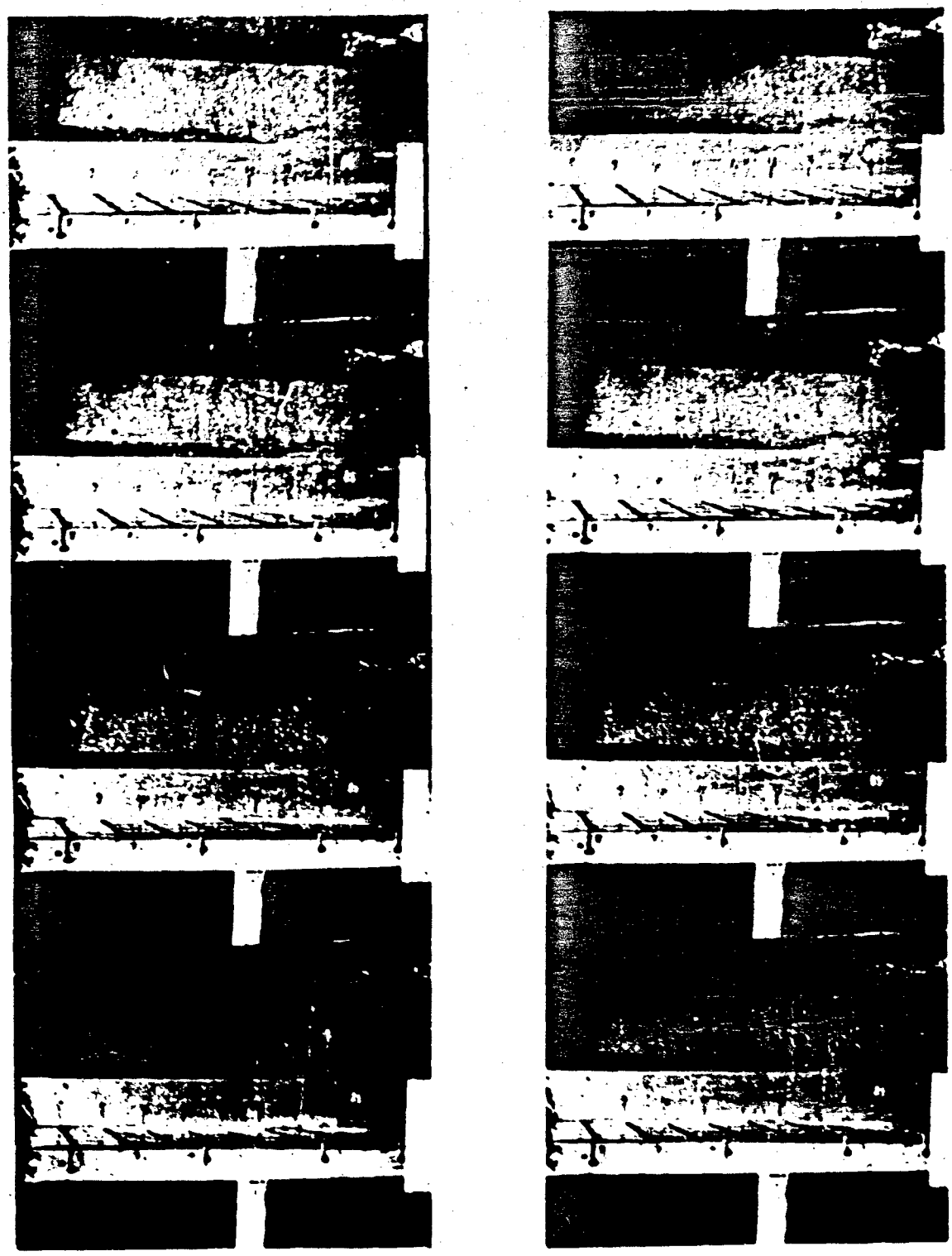

High α Free
Setting 5.0
Run 40 Film 3
$c + U \approx 35$ ft/sec, $\lambda \approx 30$ in

Fig.12b Movie Film

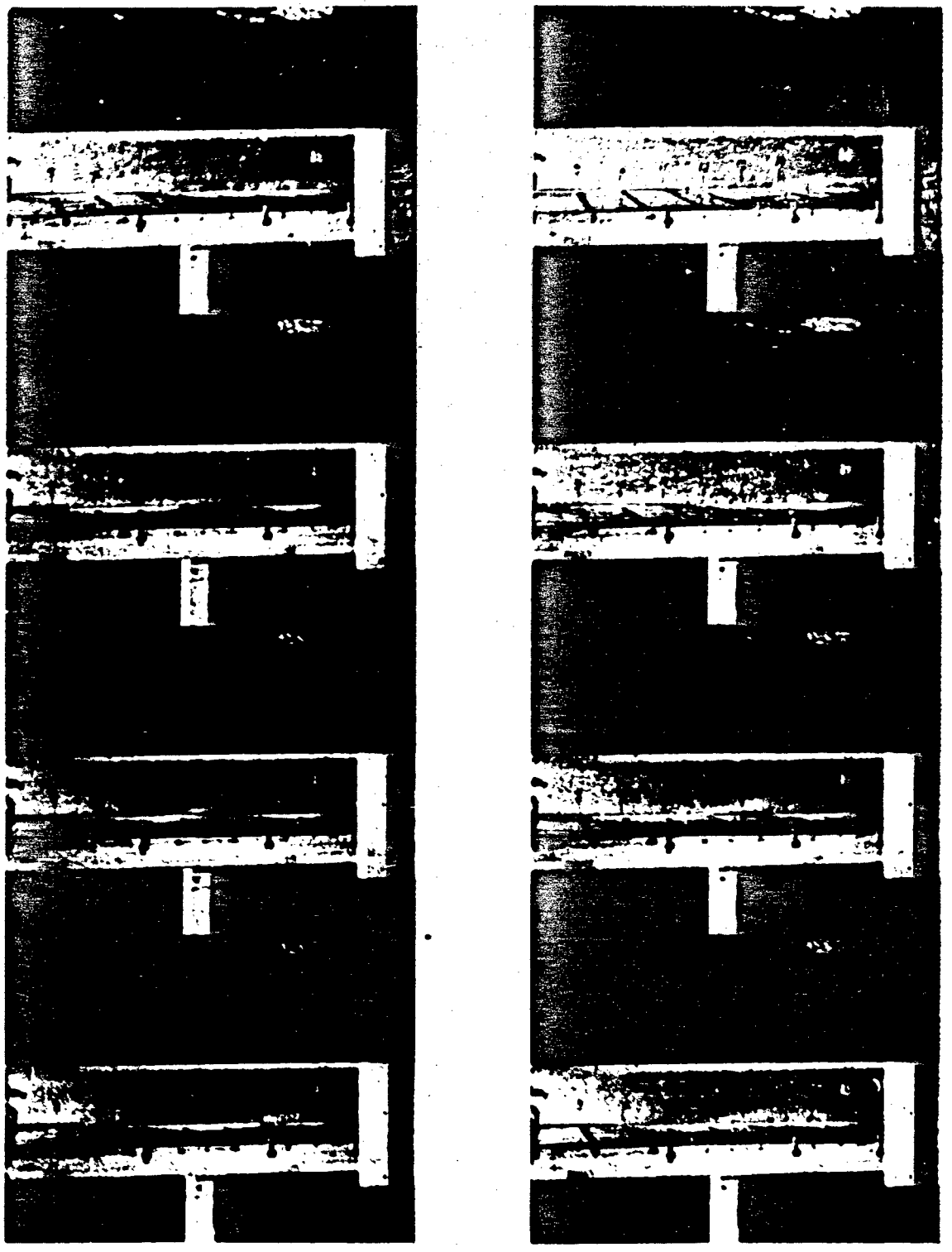

High α Pinned
Setting 5.0
Run 86, Film 6
c + U ≈ 32 ft/sec, λ ≈ 27 in

Fig.12c Movie Film

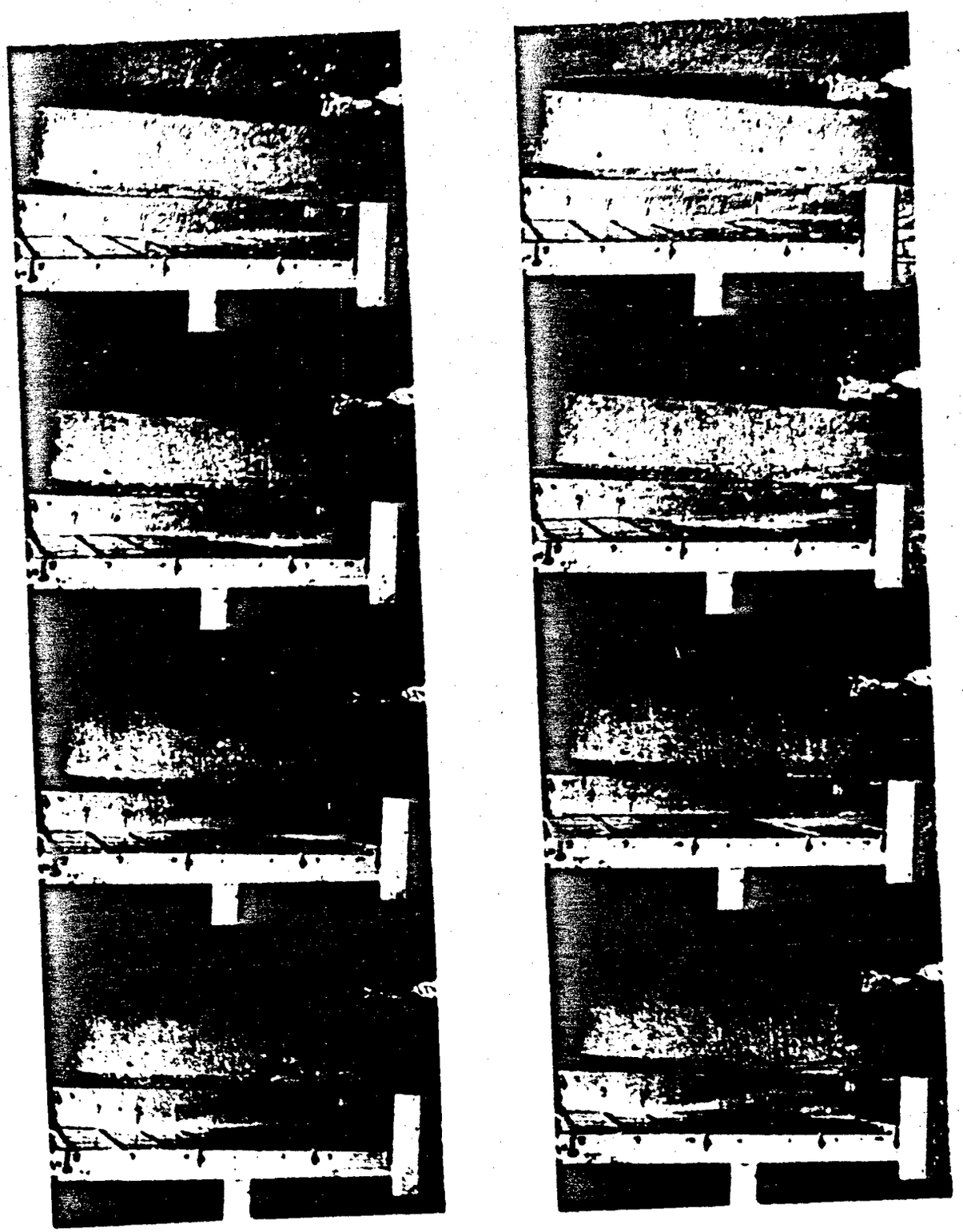

Med. α Free
Setting 5.6
Run 33 Film 10
$c + U \approx 35$ ft/sec, $\lambda \approx 30$ in

Fig.12d Movie Film

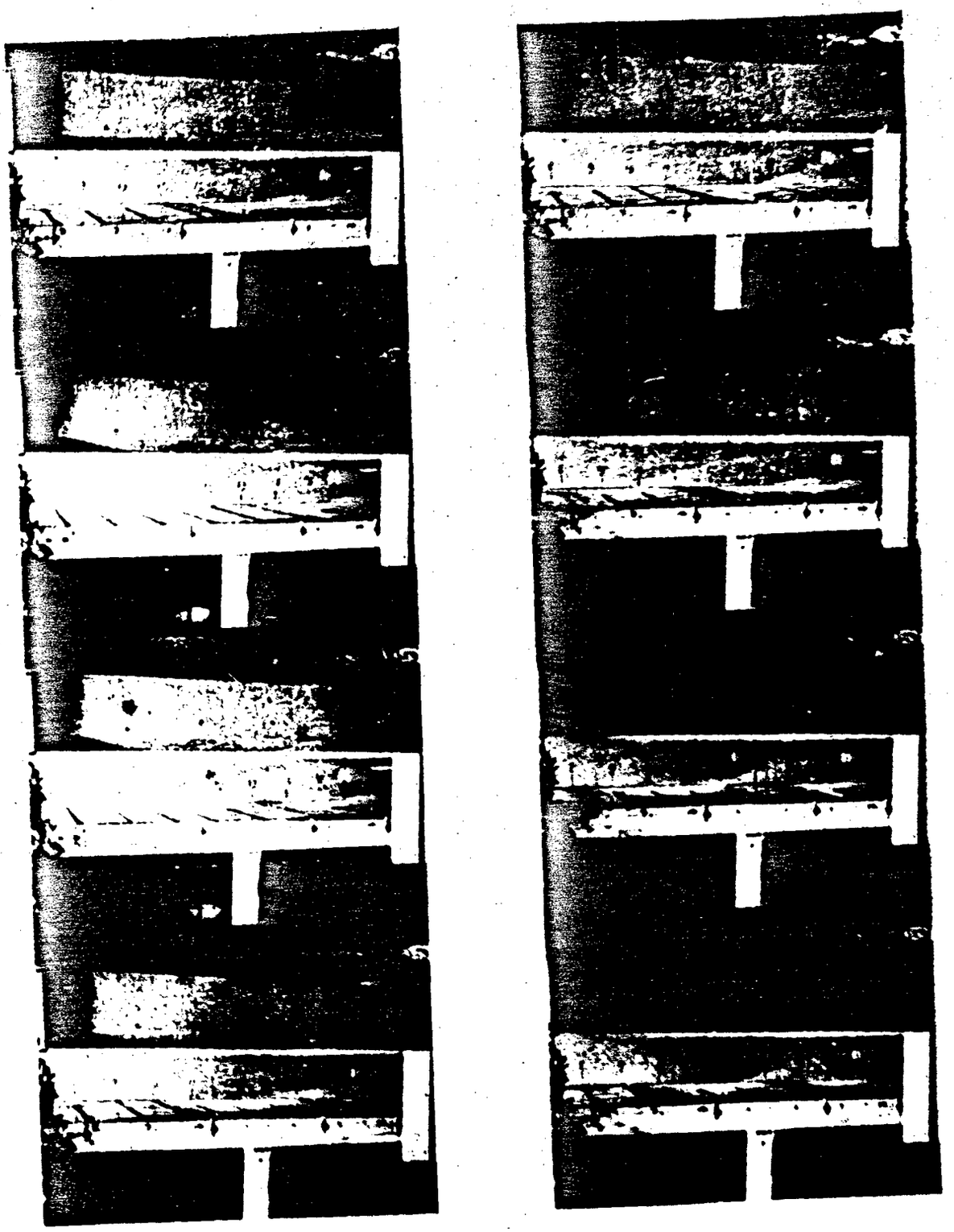

Med. α Pinned
Setting 6.8
Run 79 Film 18
c + U ≈ 32 ft/sec, λ ≈ 30 in

Fig. 12e Movie Film

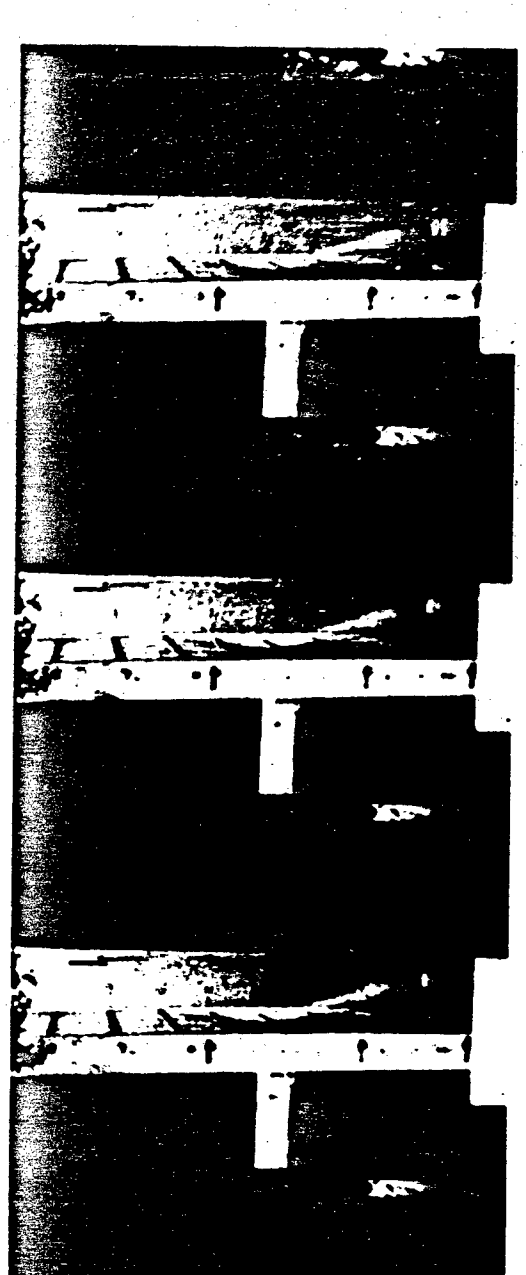

Low α Pinned
Setting 8.0
Run 121 Film 22
Static Divergence, $\lambda \approx 25$ in

Fig.13a,b Oscillograph Records

(a)

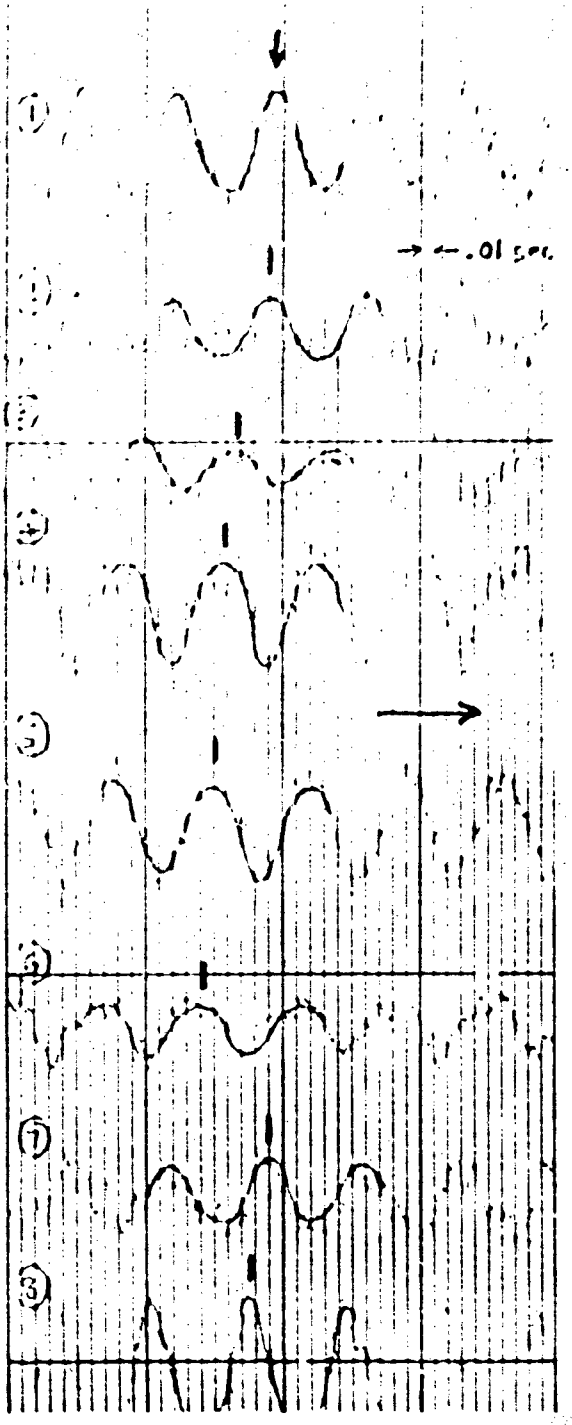

High α — Free
Setting 5.0
Run 40 Film 3
A.F. = 1
ω = 14.3 cps

(b)

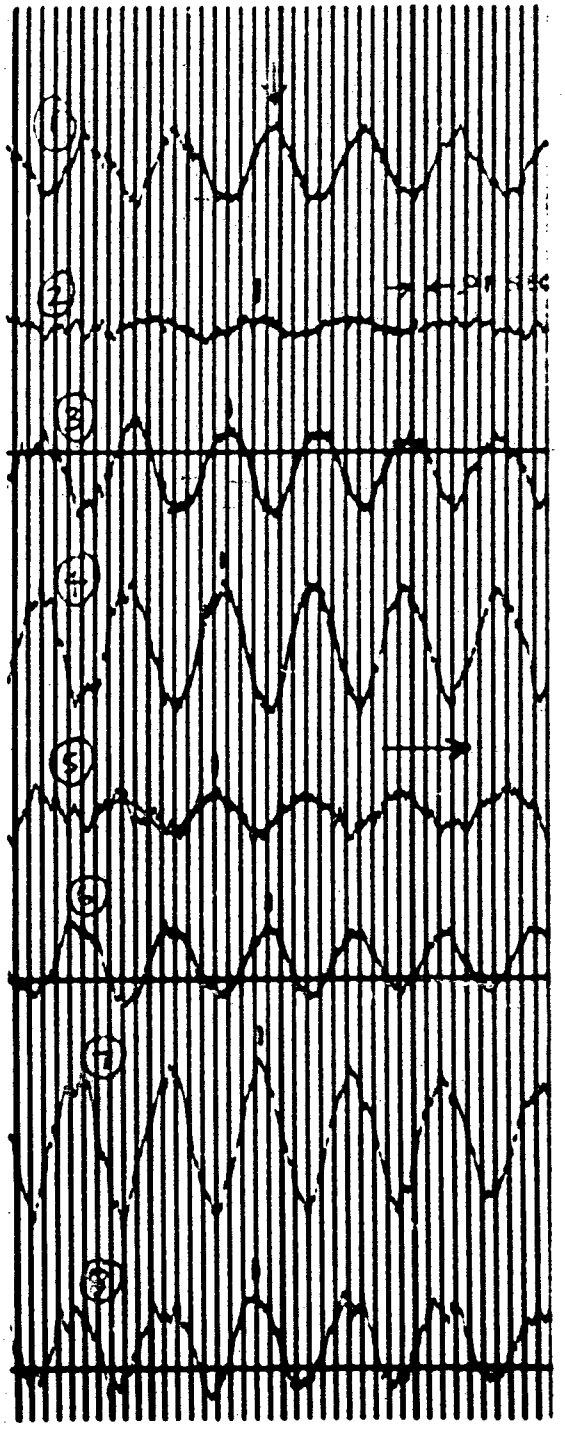

High α Pinned
Setting 5.0
Run 86 Film 6
A.F. = 1/3
ω = 14.5 cps

Fig. 13c,d Oscillograph Records

(c)

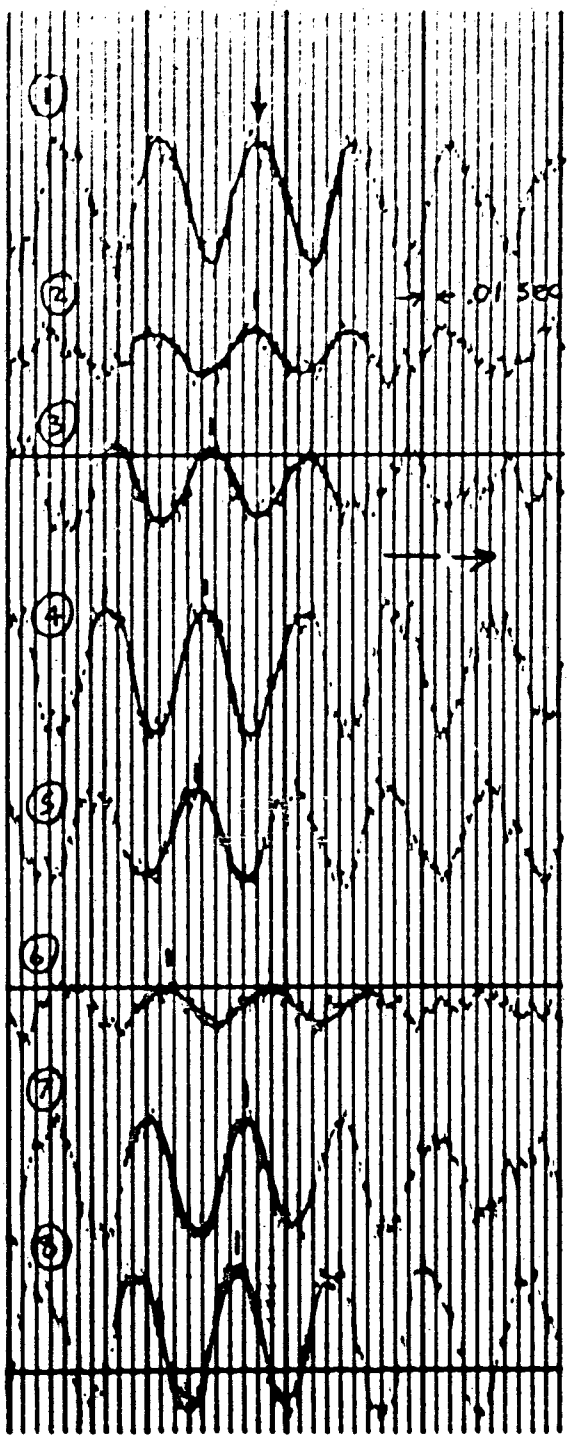

Med α Free
Setting 5.6
Run 33 Film 10
A.F. = 1
ω = 14.0 cps

(d)

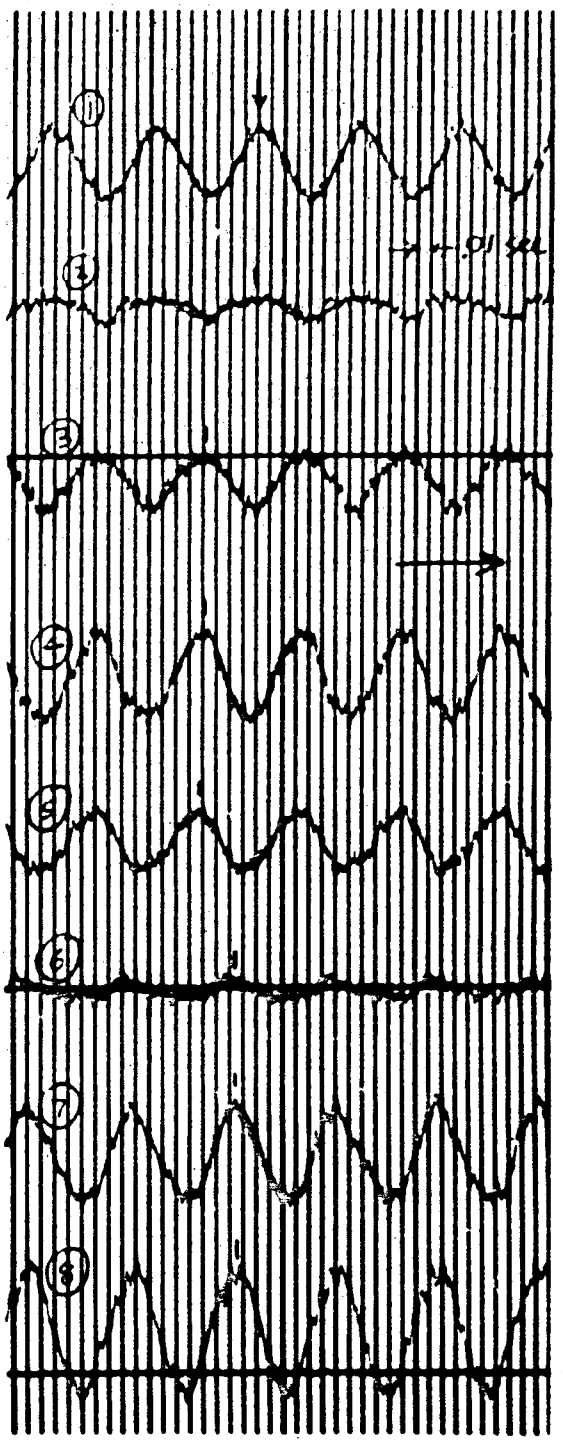

Med α Pinned
Setting 6.8
Run 79 Film 18
A.F. = 2
ω = 13.4 cps

Fig. 13c, f Oscillograph Records

(c)

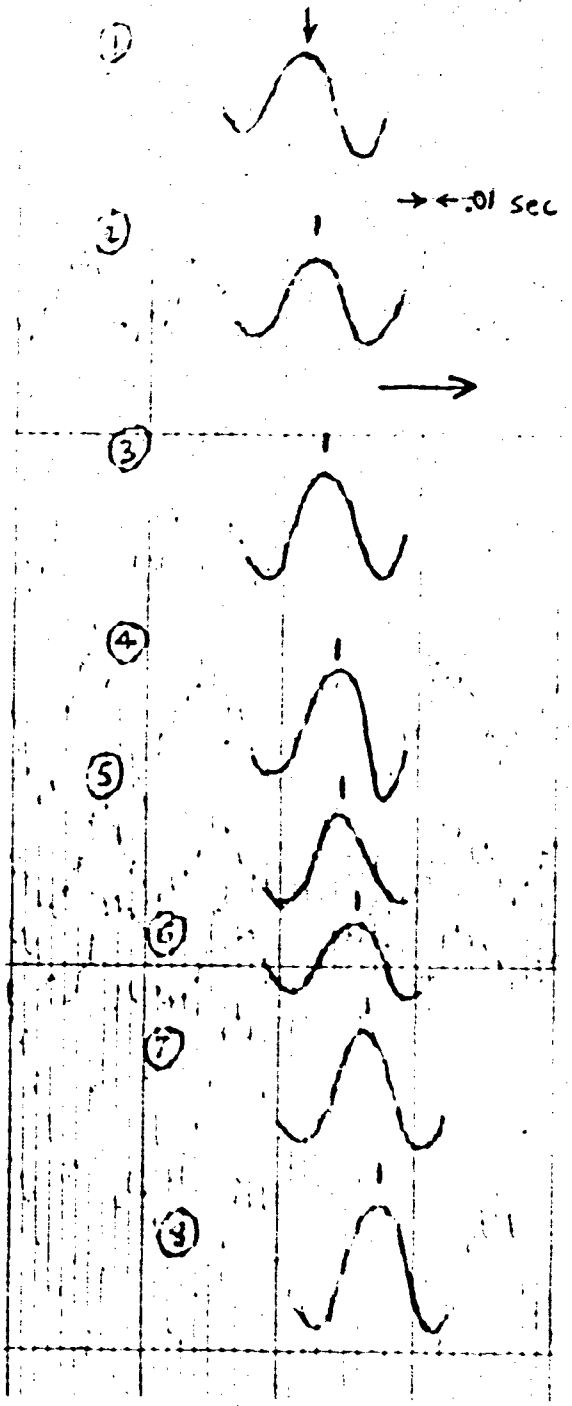

Low α Free
Setting 8.2
Run 12 Film —
A.F. = 1/3
ω = 11.8 cps
c + U = 31 ft/sec

(f)

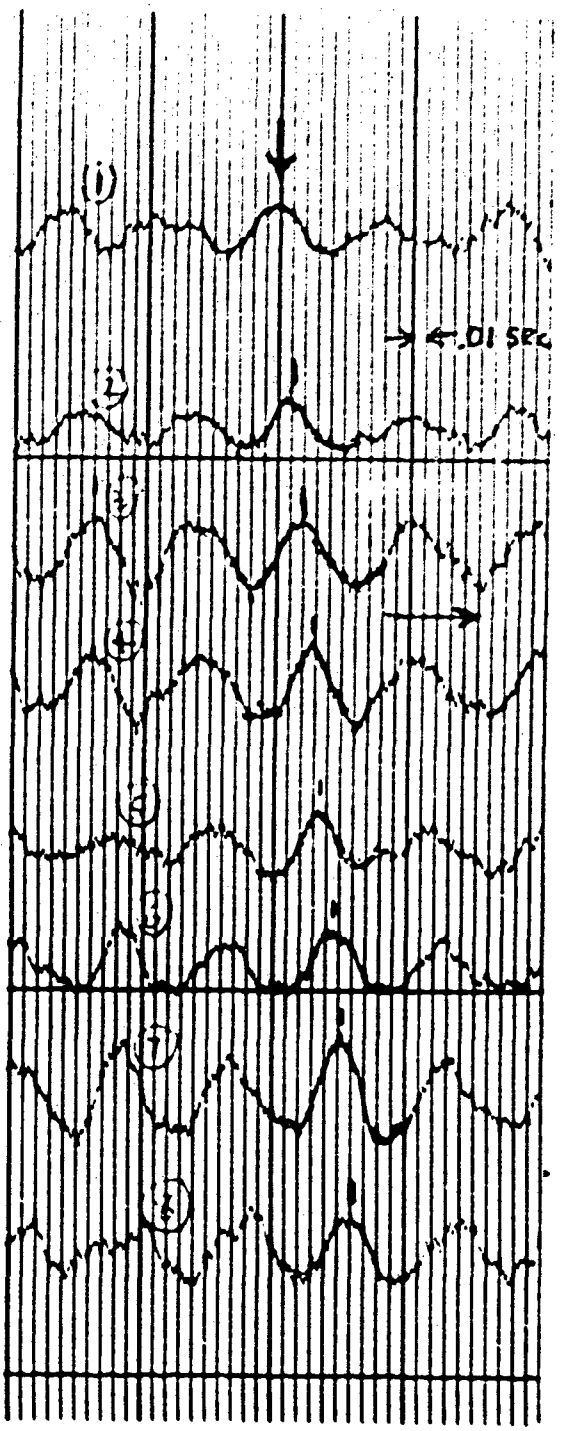

Med α Pinned
Setting 6.7
Run 76 Film —
A.F. = 1/3
ω = 12.5 cps
c + U = 31 ft/sec

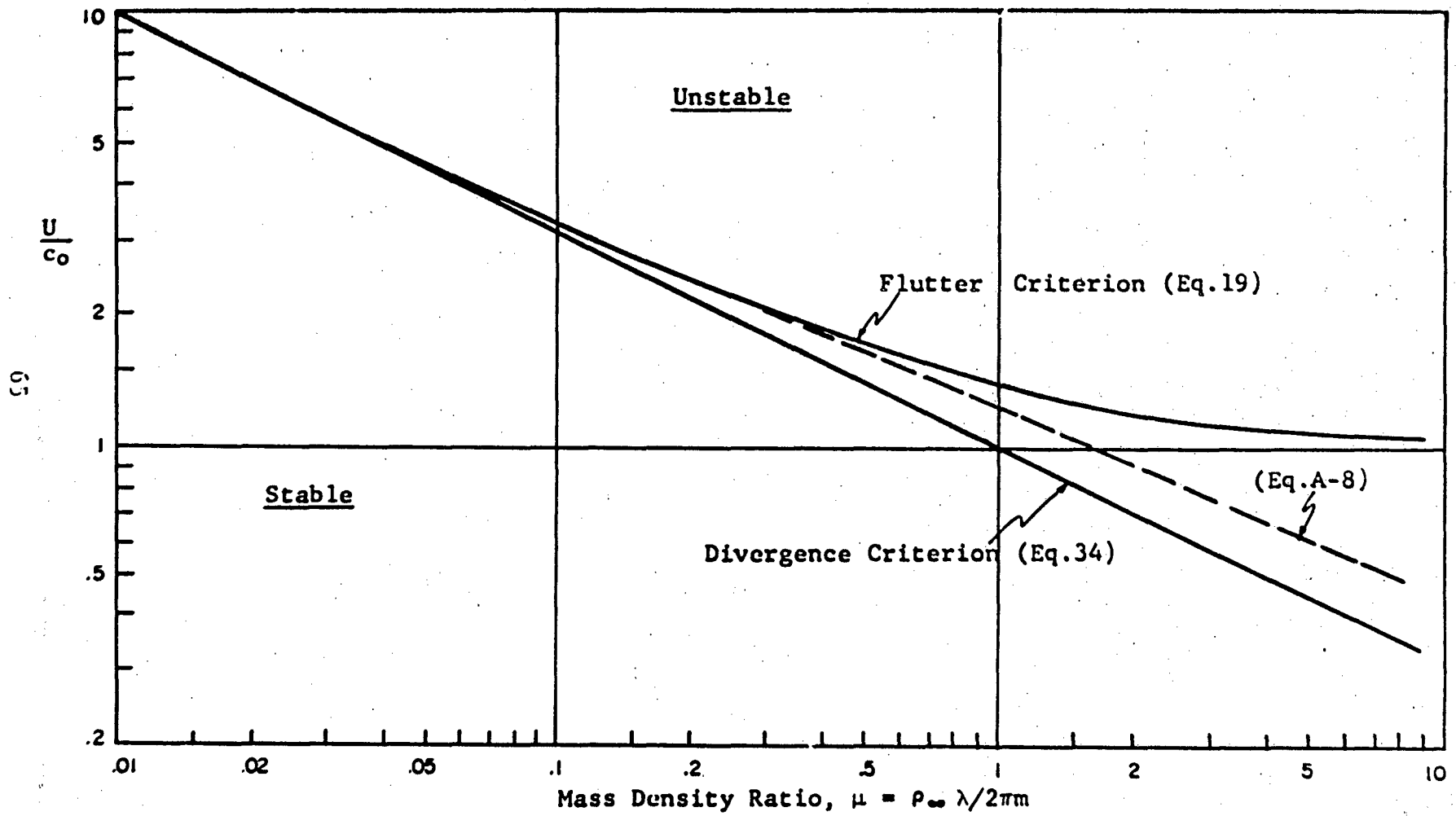

Fig.14 Flutter and Divergence Criteria (Infinite Panel)

Fig.15 c_o versus λ (Infinite Panel)

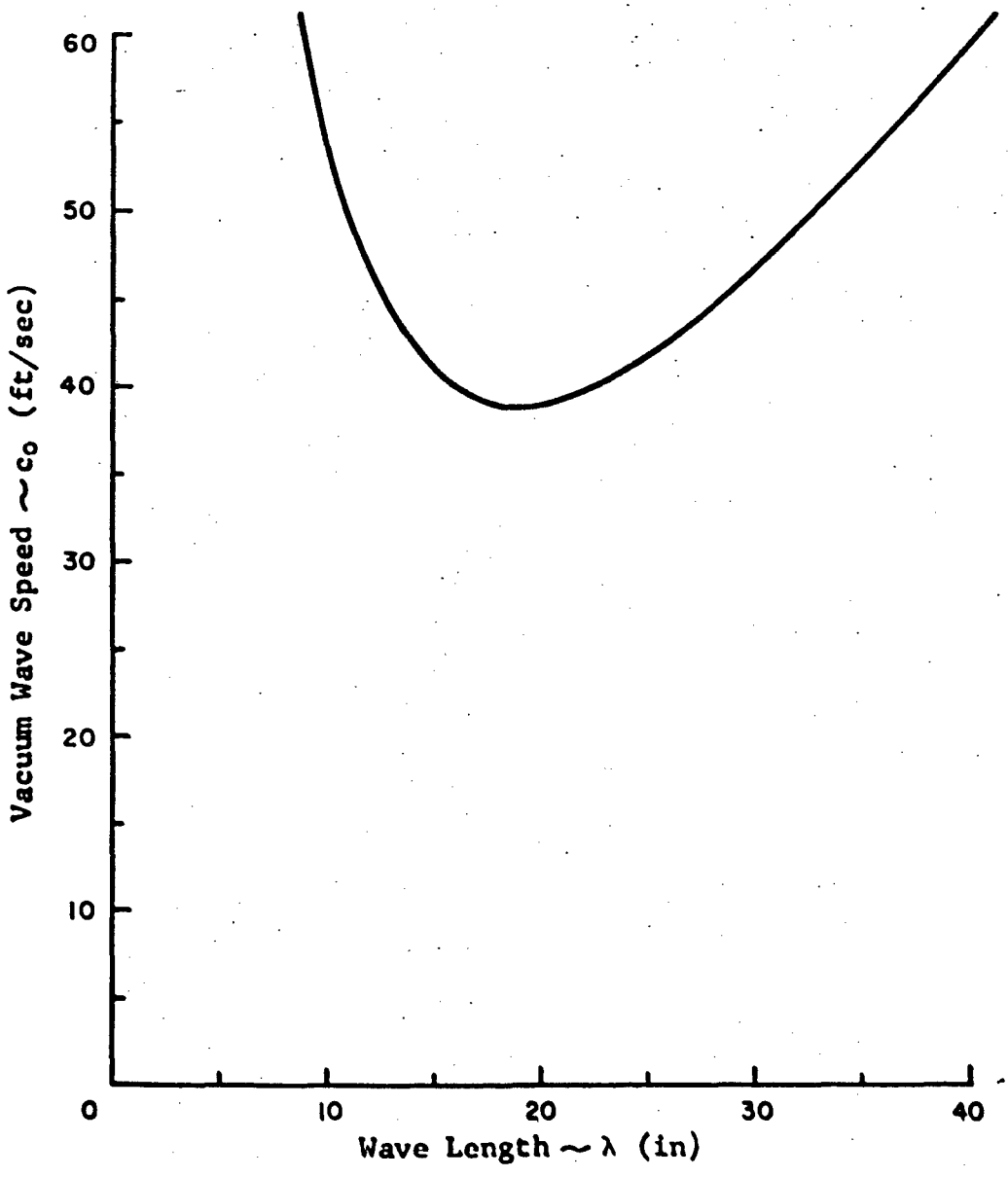

Fig.16 Flutter and Divergence Speed Versus λ
(Infinite Panel)

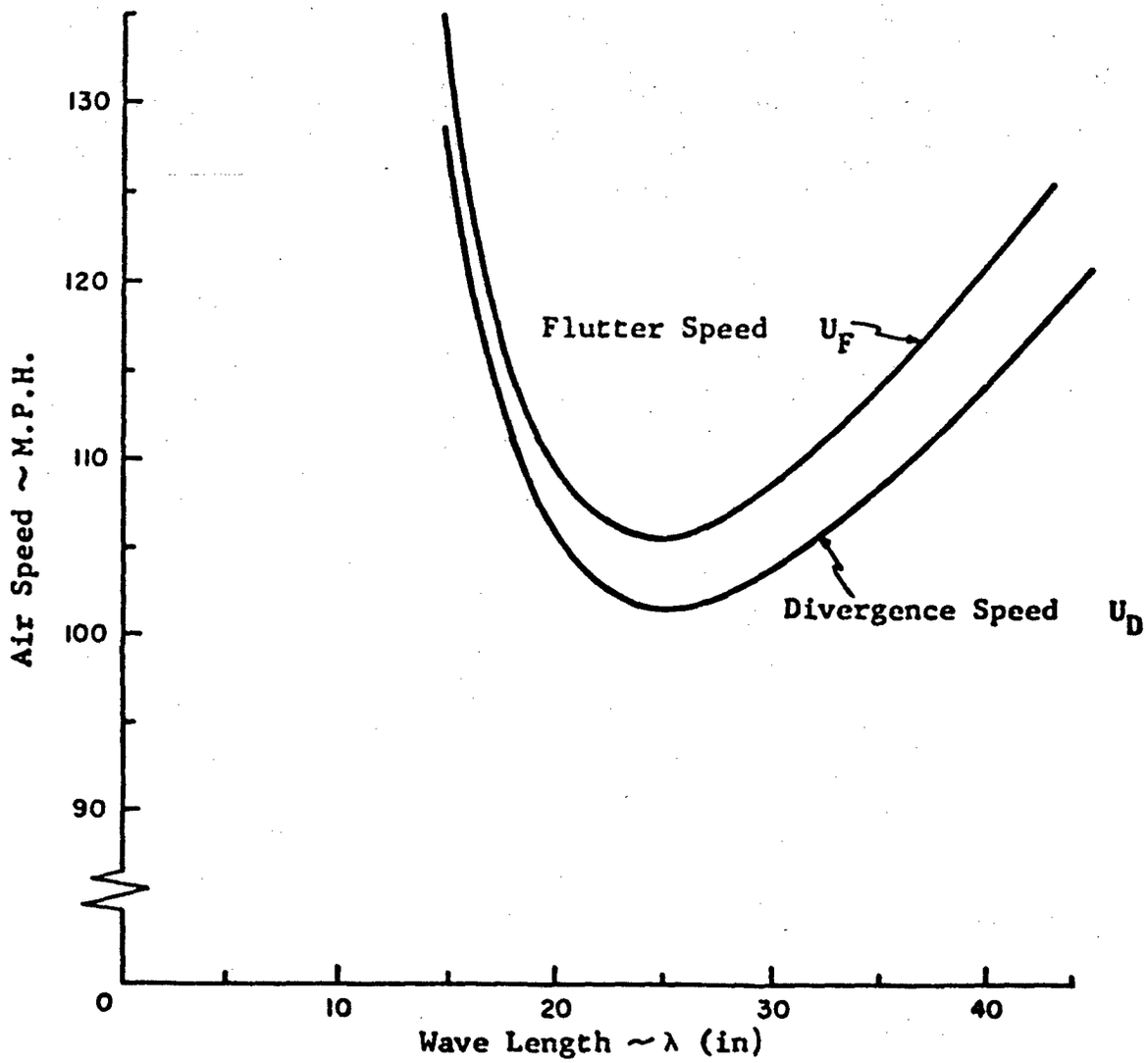

Fig.17 Wave Speed c + U for Undamped Panel (Infinite Panel)

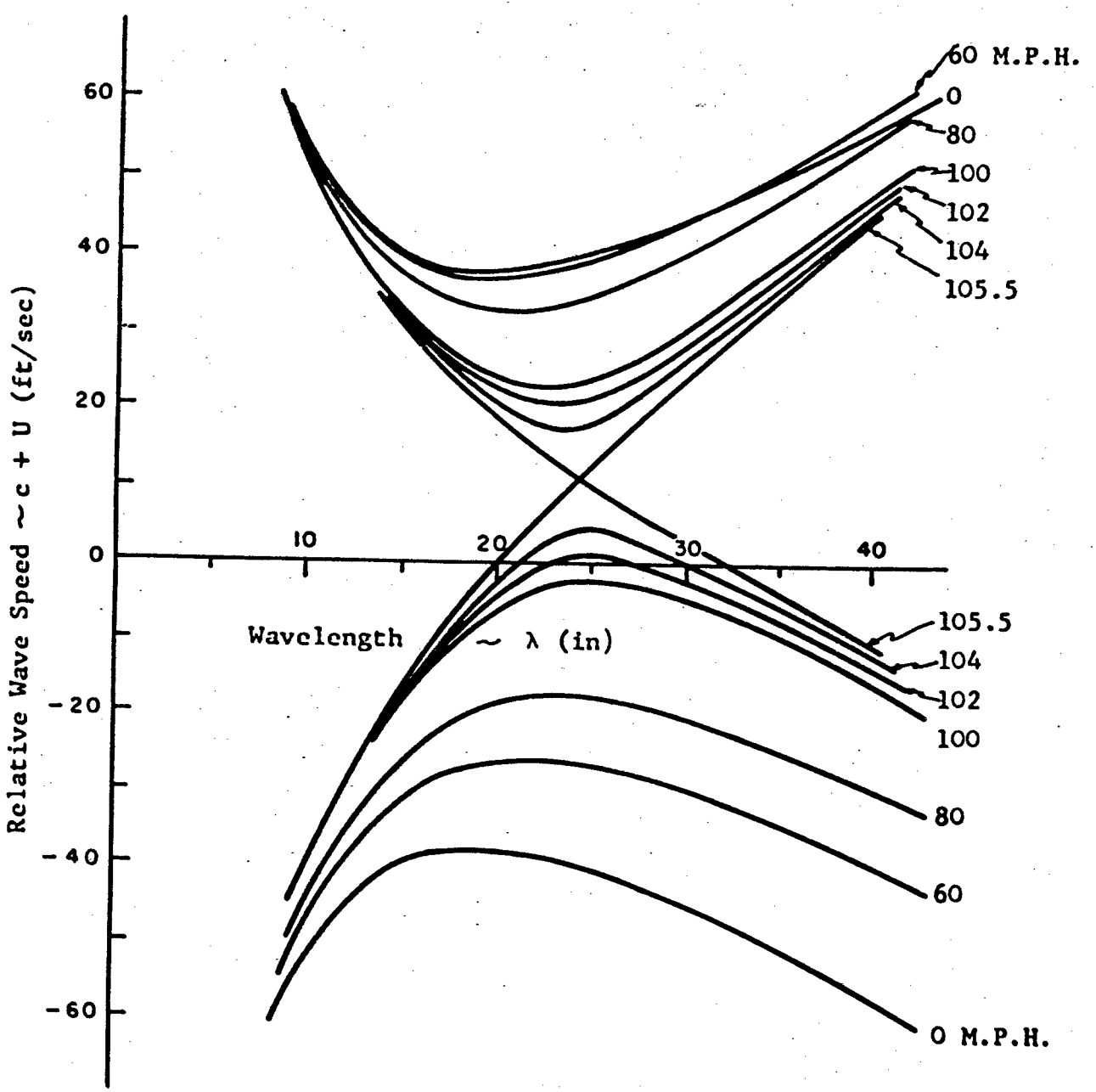

Fig.18 Complex Wave Speed c + U for Undamped Panel (Infinite Panel)

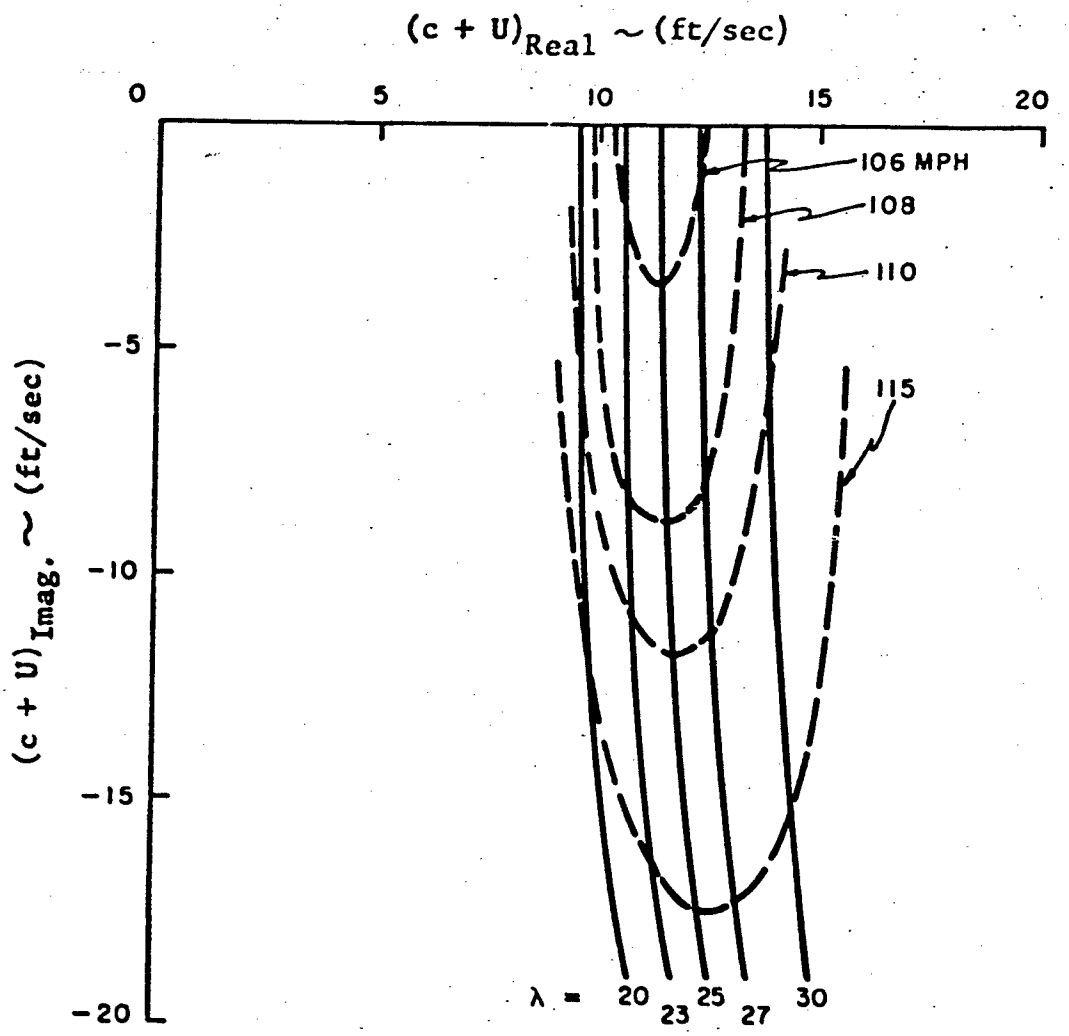

Fig.19 Amplification for Undamped Panel (Infinite Panel)

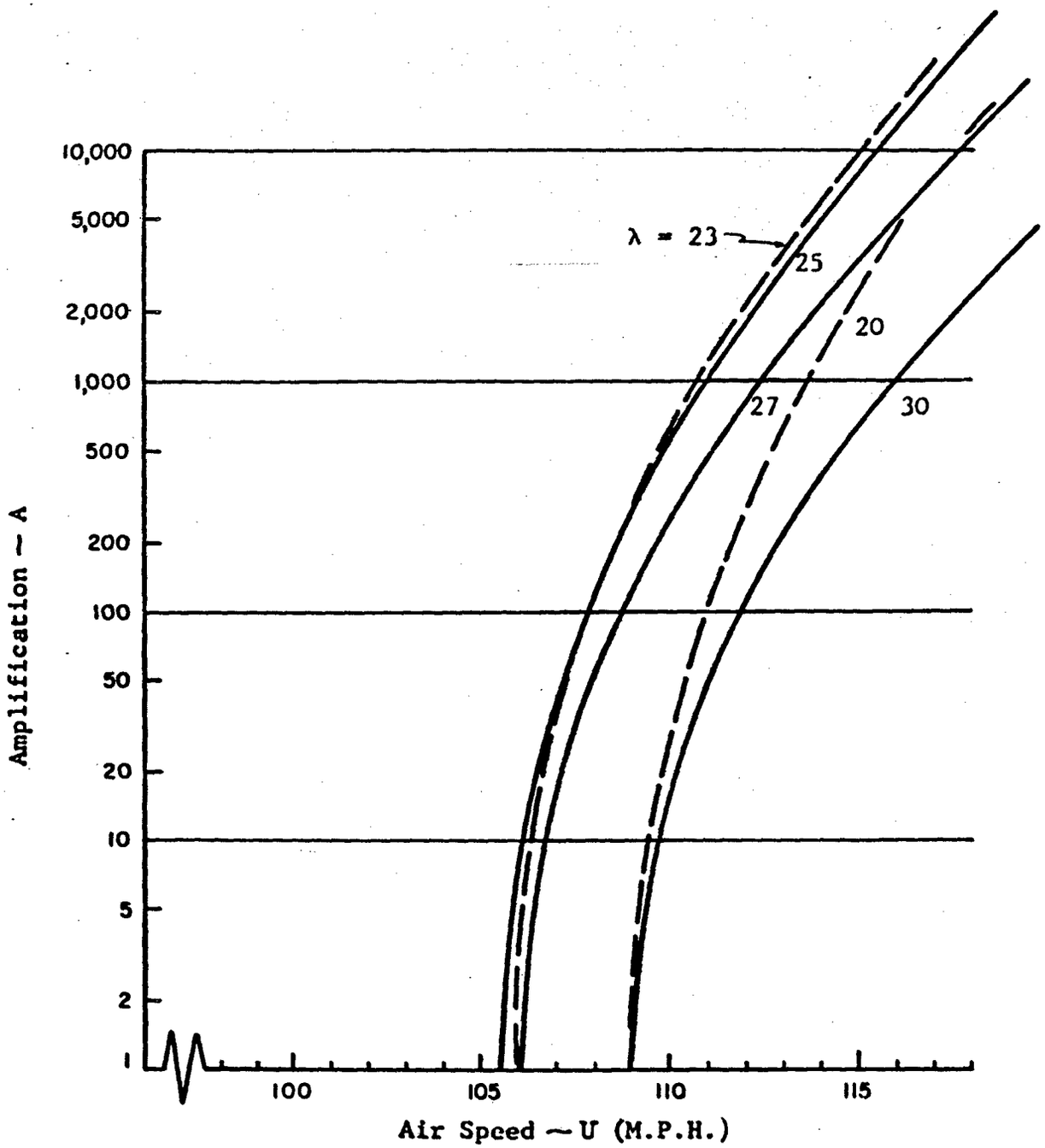

Fig.20 Complex Wave Speed c + U for Damped Panel (Infinite Panel)

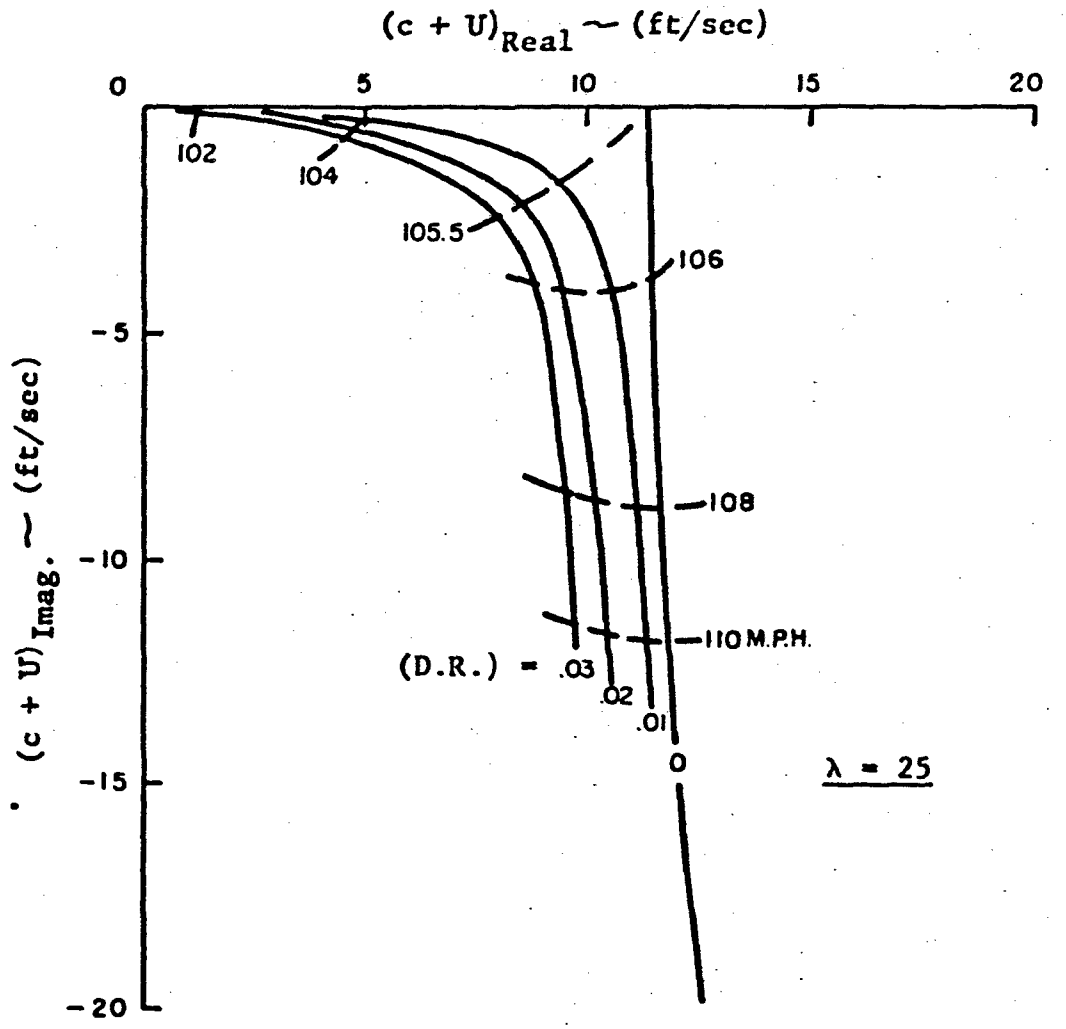

Fig.21 Amplification for Damped Panel (Infinite Panel)

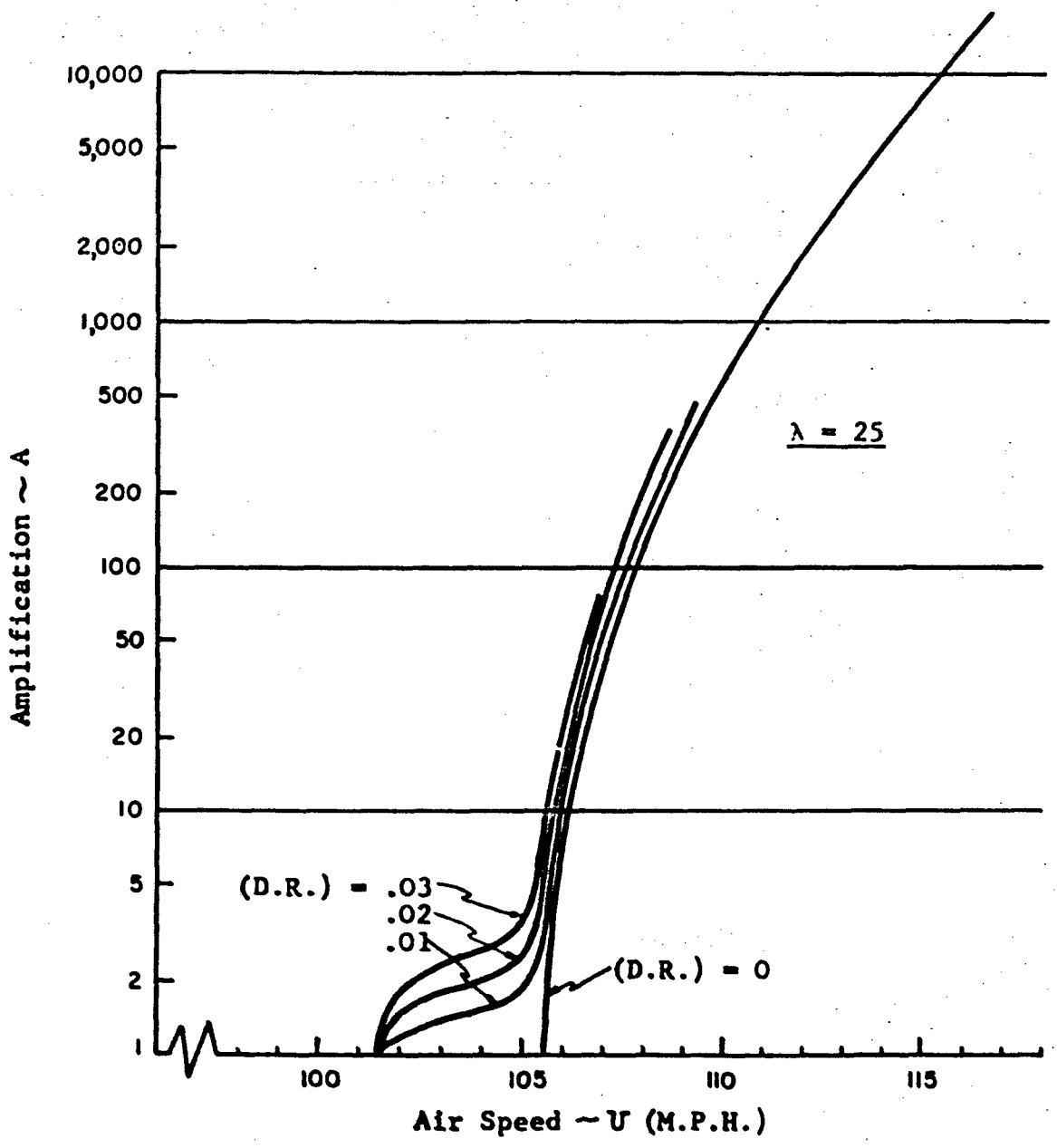

Fig.22 Divergence Behavior (Finite Panel)

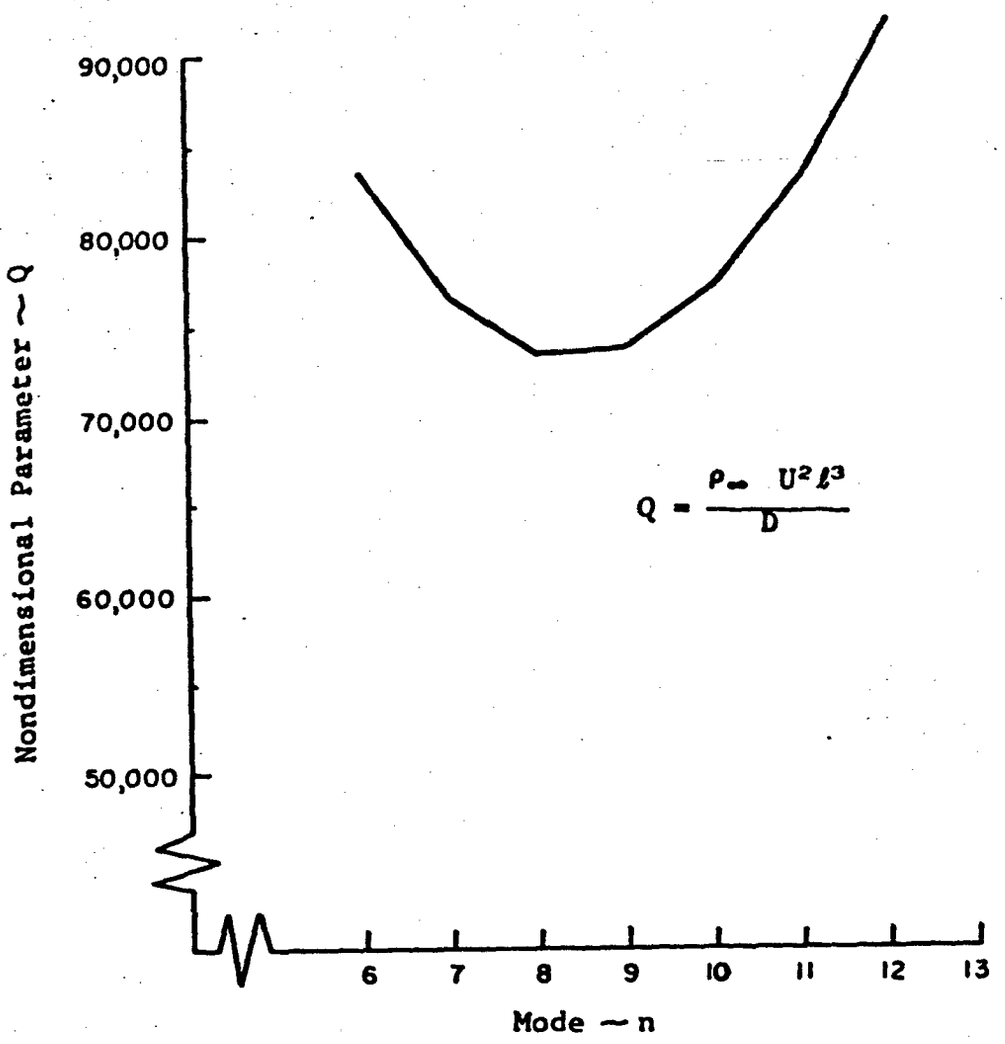

Fig. 23 Roots vs. Speed (Finite Panel)

Speed ~ U (M.P.H.)	Roots ~ S (1/sec.)		
0	±118.9 i	±127.1 i	
70.0	± 75.4 i	±105.1 i	
91.7	± 37.4 i	± 75.4 i	
99.0	± 13.9 i	± 54.8 i	
101.55	0	± 42.6 i	
101.61	±.67	± 42.3 i	Divergence
101.66	±.78	± 42.0 i	
101.71	±.67	± 41.5 i	
101.77	0	± 41.1 i	
102.0	± 2.4 i	± 39.5 i	
102.53	± 7.5 i	± 34.8 i	
102.95	± 13.0 i	± 29.4 i	
103.13	± 21.3 i	± 21.3 i	
103.28	± .6 ± 21.3 i		Flutter
103.96	±15.2 ± 21.4 i		
105.50	±26.1 ± 21.7 i		
107.0	±33.6 ± 22.0 i		
108.0	±37.8 ± 22.2 i		

Fig.24 Amplification(Finite Panel)

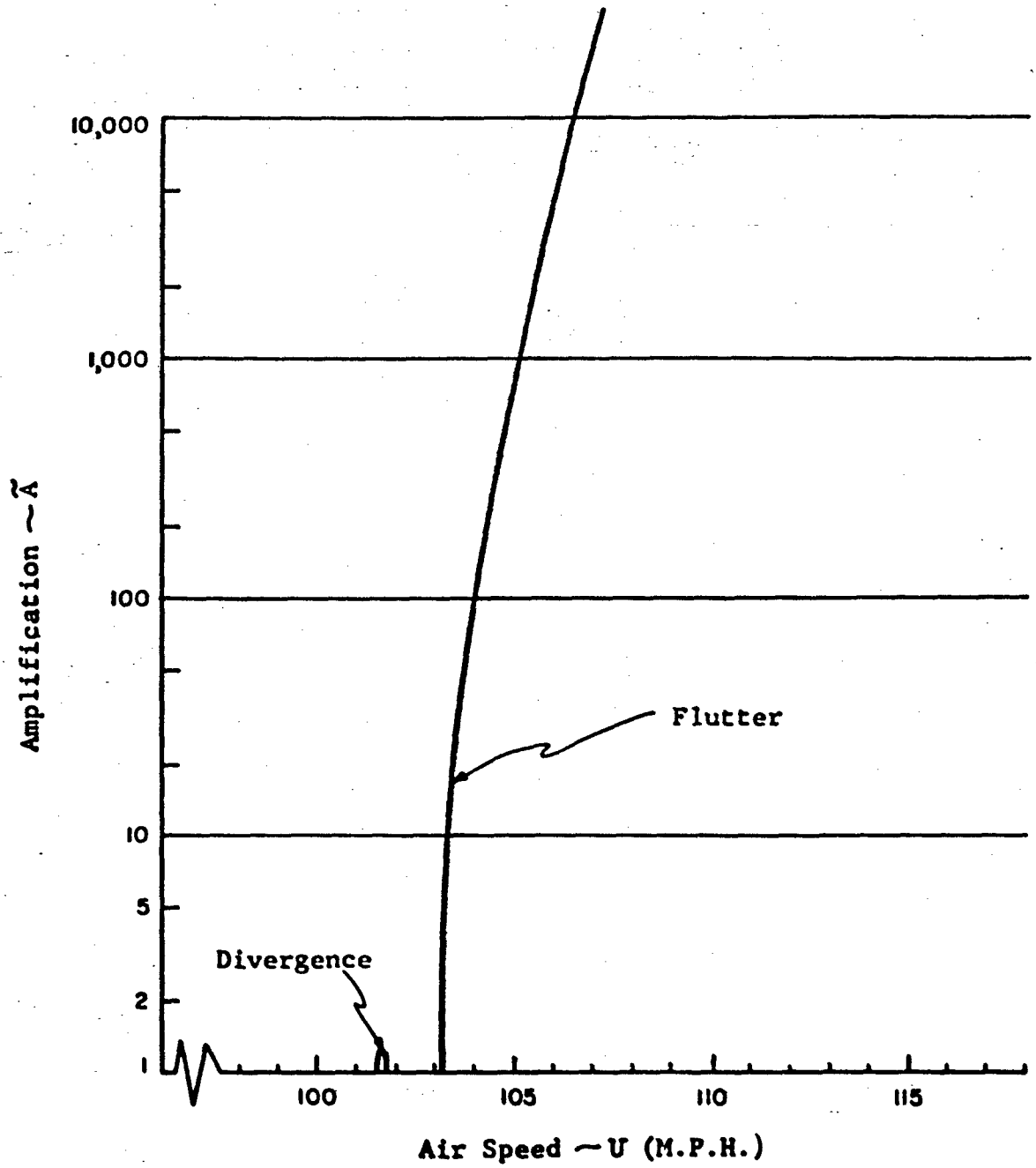

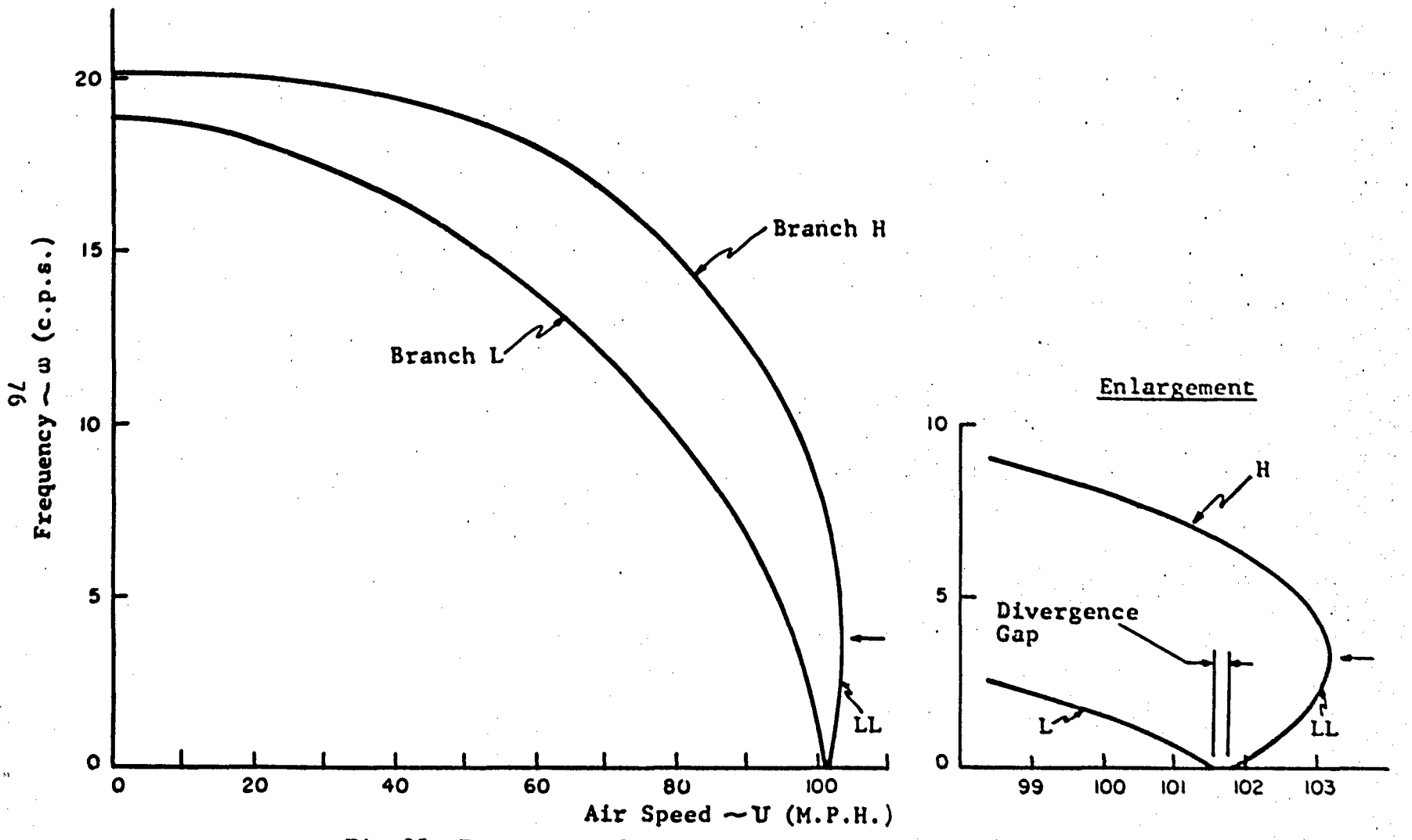

Fig.25 Frequency of Steady Oscillations (Finite Panel)

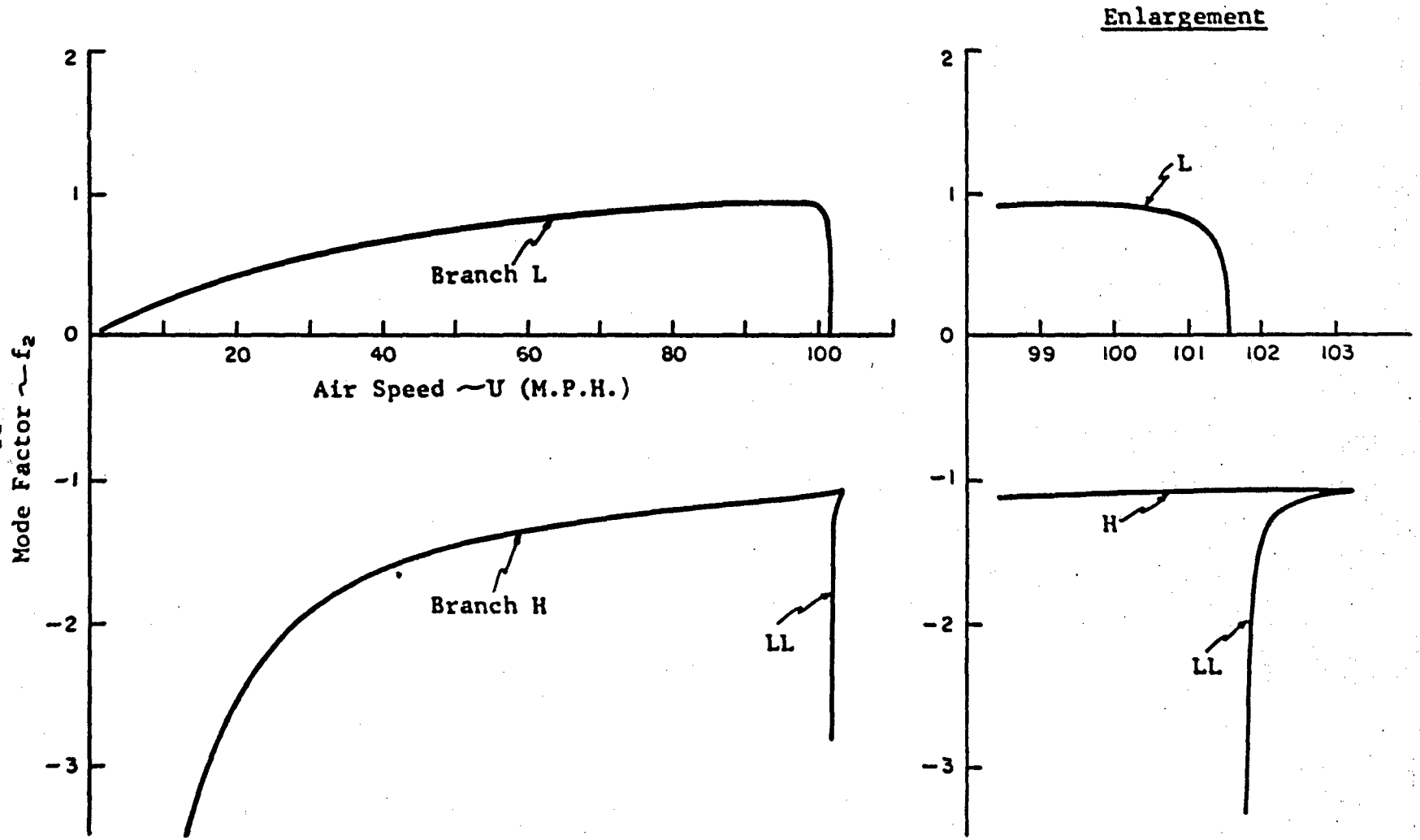

Fig.26 Mode Factor f_2 (Finite Panel)

Fig.27 Oscillations at Flutter (Finite Panel)

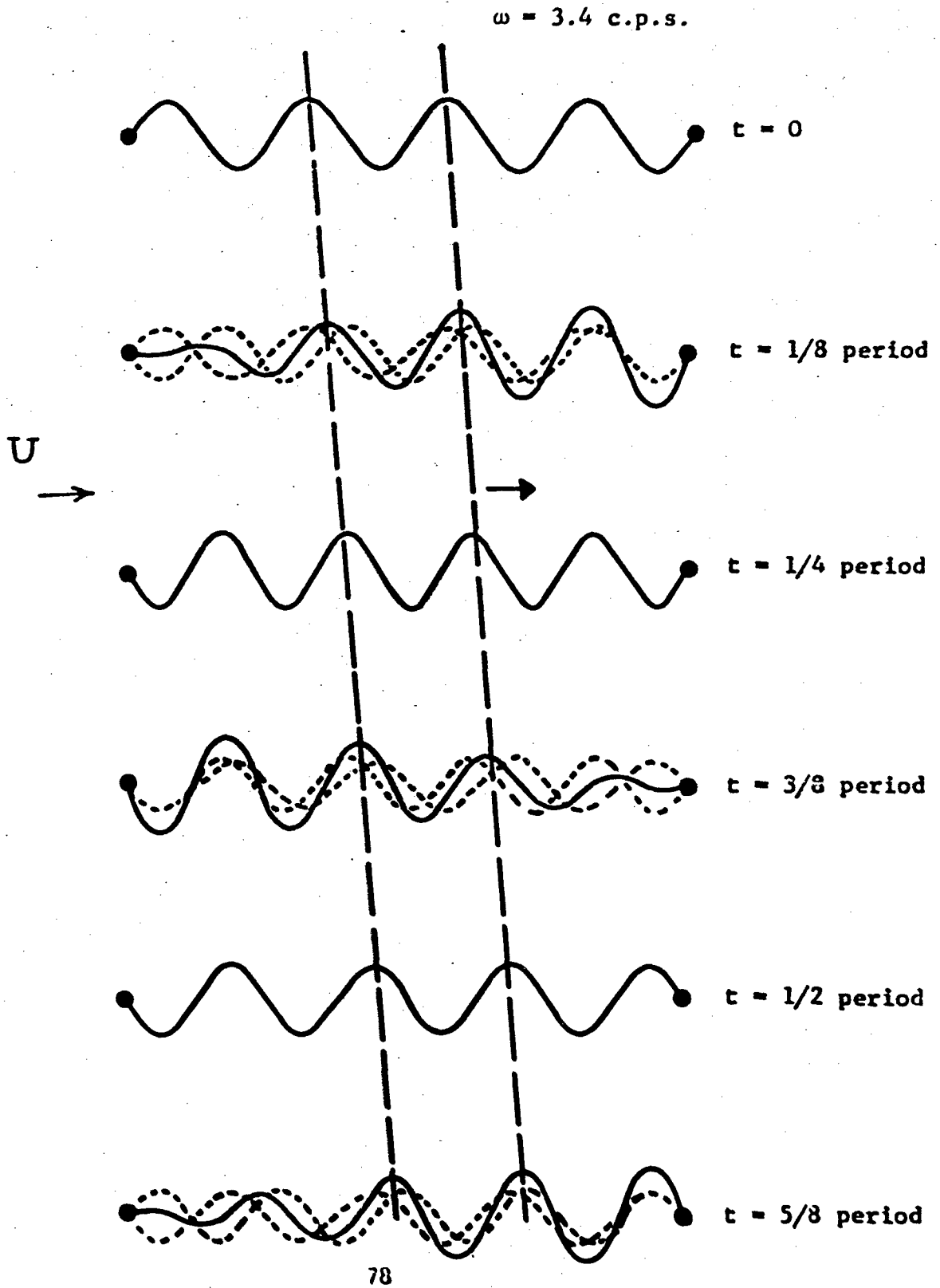

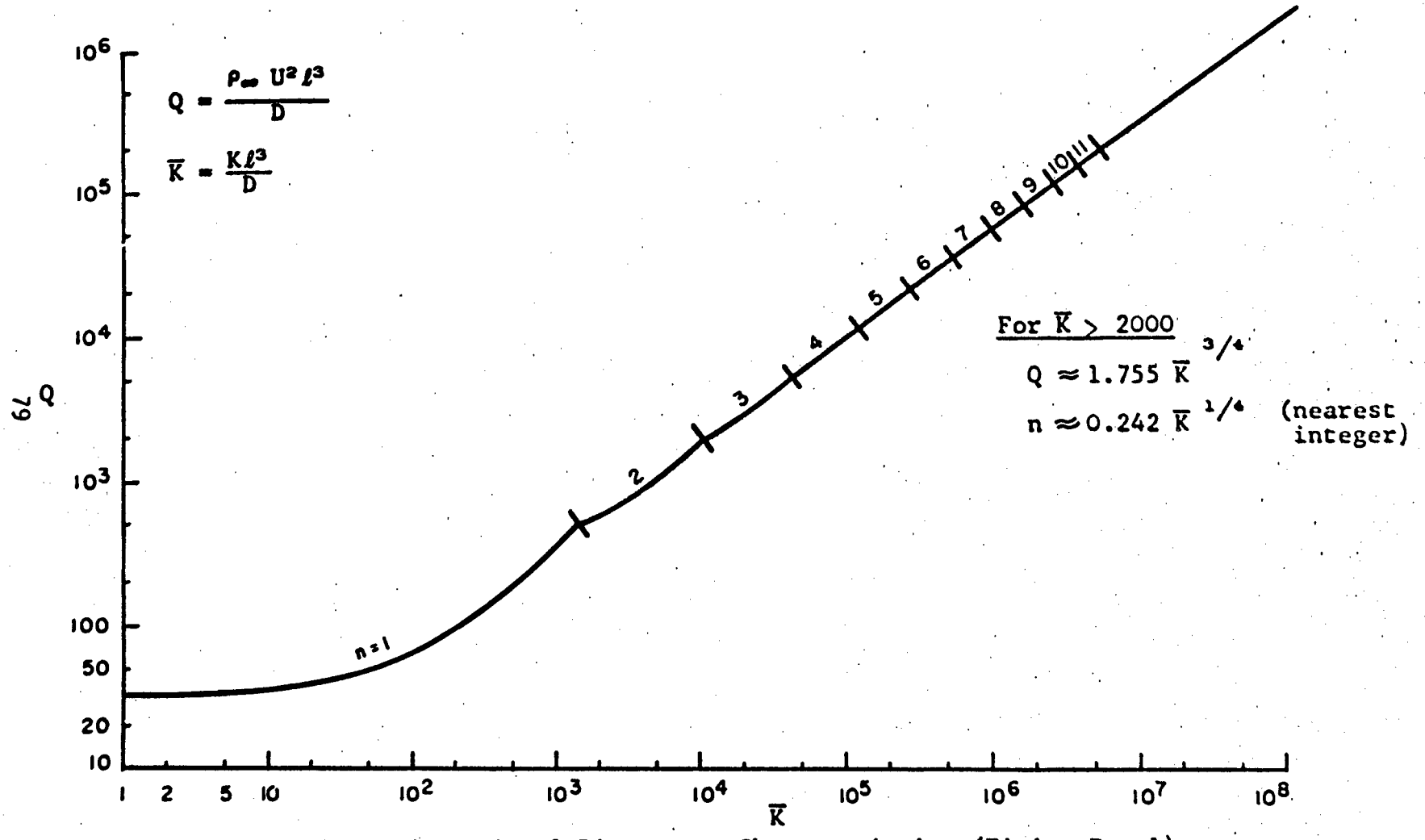

Fig.28 Nondimensional Divergence Characteristics (Finite Panel)